Clays and Clay Minerals, Vol. 64, No. 4, 348–373, 2016.

INVESTIGATION OF THE INTERLAYER ORGANIZATION OF WATER AND IONS IN SMECTITE FROM THE COMBINED USE OF DIFFRACTION EXPERIMENTS AND MOLECULAR SIMULATIONS. A REVIEW OF METHODOLOGY, APPLICATIONS, AND PERSPECTIVES

Eric Ferrage*
Université de Poitiers, CNRS, UMR 7285 IC2MP, Equipe Hydrasa, 5 rue Albert Turpain, Bât. B8, TSA 51106, 86073 Poitiers cedex 9, France

Abstract—Investigation of the organization of interlayer water and cations in smectite is a permanent topic in clay science for environmental science, civil engineering, materials science, and industrial applications. Experimental X-ray (or neutron) diffraction methods and molecular simulations are key techniques to probe the organization of the smectite structure at a similar molecular length scale. The combination of both of these experimental and numerical methods represents a complementary approach to reveal the structural heterogeneity of real samples, design and model a wide range of smectite structures, and validate the simulation results through comparison with experimental data.

This paper first revisits establishment of the original interlayer model as developed in the 1930s for the organization of water and ions in the smectite structure using X-ray diffraction (XRD) techniques. Then, based on a simplified approach, key theoretical tools are provided to calculate XRD pattern 00*l* reflections for a periodic smectite structure with a wide range of interlayer compositions and organizations using conventional spreadsheet software. In addition to educational purposes, this theoretical description is used to describe the principal parameters governing the positions and intensities of experimental XRD 00*l* reflections. This calculation toolbox is also used to determine better the layer-to-layer distances considered in molecular simulations and to validate these simulations through a detailed collation procedure using experimental data.

Recent examples of the application of such a procedure to collate experimental diffraction data and molecular simulations are presented for the specific case of deciphering the molecular organization of interlayer water and cations in the different smectite hydrates (mono-, bi-, and tri-hydrated layers). The extension of this approach to the interlayer refinement of organo-clays is also detailed, and perspectives regarding the characterization of other lamellar compounds are discussed.

Key Words—Interlayer Ion Organization, Interlayer Water Organization, Molecular Simulation, Neutron Diffraction, Smectites, X-ray Diffraction.

INTRODUCTION

Smectites are ubiquitous clay minerals in Earth's surface environments, where the minerals display a wide range of crystal-chemistry properties. The crystal structure is composed of a 2:1 layer consisting of an octahedral sheet (with Al^{3+}, Mg^{2+}, Fe^{2+}, Fe^{3+}, and Li^{+}, among others) sandwiched between two opposing tetrahedral sheets (with Si^{4+}, Al^{3+}, and Fe^{3+}, Figure 1; Brigatti *et al.*, 2006). Isomorphic substitutions in both the tetrahedral or octahedral sheets induce a permanent layer charge deficit, compensated by the presence of exchangeable cations in the interlayer space. The high cation exchange capacity and minute crystal size of smectites leads to a high specific surface area and the pivotal role that smectites play in controlling pollutant behavior in natural media (Tertre *et al.*, 2011a; Akai *et al.*, 2013; Dzene *et al.*, 2015; and references therein). This sorption property also makes smectite a promising natural buffer to inhibit the migration of pollutants in disposal facilities for hazardous wastes worldwide (including high-level activity nuclear wastes; Madsen, 1998; Gates *et al.*, 2009).

The hydration properties of the interlayer cations are also responsible for the well known stepwise expansion of the layer-to-layer distance (*i.e.* d_{001}) in the smectite structure with increasing water activity. This sequential expansion is commonly described as resulting from the incorporation of 1 to 3 planes of interlayer water molecules (Figure 1), leading to the mono-hydrated (1W, d_{001} = 11.8–12.9 Å), bi-hydrated (2W, d_{001} = 14.5–15.8 Å), and tri-hydrated (3W, d_{001} = 18.0–19.5 Å) states, in addition to the dehydrated state (0W, d_{001} = 9.6–10.7 Å). The swelling/collapsing behavior resulting from the hydration/dehydration pro-

* E-mail address of corresponding author:
eric.ferrage@univ-poitiers.fr
DOI: 10.1346/CCMN.2016.0640401

This paper is published as part of a special issue on the subject of 'Computational Molecular Modeling'. Some of the papers were presented during the 2015 Clay Minerals Society-Euroclay Conference held in Edinburgh, UK.

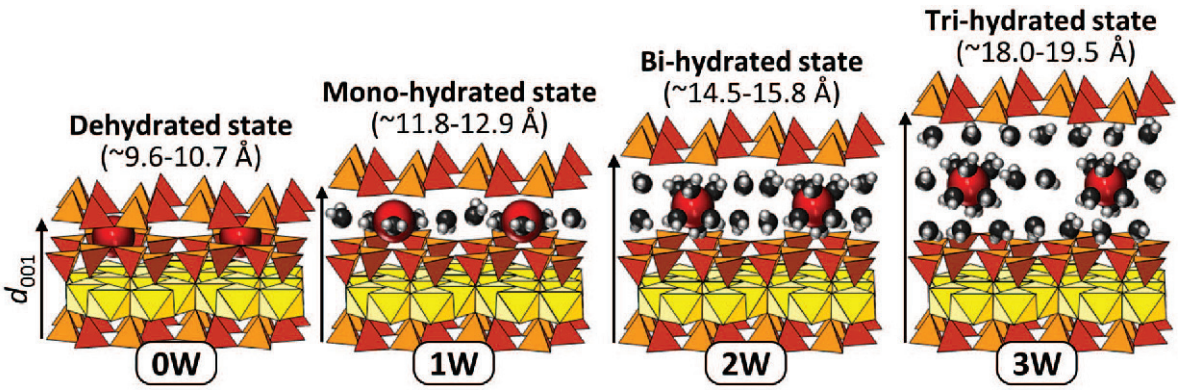

Figure 1. Schematized representation of crystal structure for the different smectite hydration states and the ranges of layer-to-layer distances (d_{001}): dehydrated state ($d_{001} \approx 9.6-10.7$ Å), mono-hydrated state ($d_{001} \approx 11.8-12.9$ Å), bi-hydrated state ($d_{001} \approx 14.5-15.8$ Å), and tri-hydrated state ($d_{001} \approx 18.0-19.5$ Å).

cess is the underlying mechanism of numerous problems in civil engineering and soil science. This behavior is related to the shrinkage effect, which can generate additional preferential pathways for water/contaminant transfer (Tessier *et al.*, 1992; Harris *et al.*, 1994; Vasseur *et al.*, 1995).

In light of the aforementioned environmental considerations, the organization of interlayer water and ions in smectite was studied as early as the 1930s, with the emergence of the X-ray diffraction (XRD) technique (Hendricks and Fry, 1930; Hofmann *et al.*, 1933). In the early 1990s (Skipper *et al.*, 1989, 1991; Delville, 1991, 1993), this structural characterization also benefited from the development of classical molecular simulation methods. These methods typically take the form of molecular dynamics (MD) or Monte Carlo (MC) simulations. The most popular simulations are performed in the microcanonical (NVE), canonical (NVT), grand canonical (μVT), and isothermal-isobaric (NPT) ensembles, in which the variables N, V, E, T, μ, and P represent the number of particles, volume, energy, temperature, chemical potential, and pressure, respectively (Cygan *et al.*, 2009). These techniques have provided a new level of detail in the characterization of the interlayer organization of species in smectite as well as the reactivity.

Currently, experimental diffraction experiments and molecular simulations represent complementary methods for the investigation of interlayer water and ion organization in smectite. The XRD technique is particularly adapted for revealing the crystal structure disorder and actual layer-to-layer distance under various environmental conditions. Classical molecular simulations can provide a more detailed picture of the interlayer organization of water and ions compared to XRD analysis, but require combination with experimental data. This combination concerns both the choice of layer-to-layer distance to perform the simulation and potential confrontation of the computed interlayer model with experimental data.

In the scope of this special issue devoted to molecular modeling in clay minerals, the present contribution describes the methodology of combining diffraction experiments and molecular simulations for an improved description of interlayer water and ions in smectites. In the first part, emphasis is placed on the less familiar background of XRD studies of early smectite interlayer structure models and the progress made in the quantitative characterization of smectite hydration properties. In the second part of the manuscript, a simplified formalism is presented for the calculation of the XRD pattern of 00*l* reflections using conventional spreadsheet software. The third section focuses on the methodology of extraction from experimental XRD diffractograms of the layer-to-layer distance to be used in molecular simulations and on the generation of the theoretical pattern of 00*l* reflections from molecular simulation results. In the fourth part of this paper, some applications of the collation procedure between experimental and numerical data are shown for different smectite structures. This combined approach is shown to improve the description of interlayer configurations of water and ions while providing a clear asset for the validation of simulation results. Finally, some conclusions and possible larger perspectives on the use of this methodology are discussed for other lamellar compounds.

HISTORICAL PERSPECTIVE ON XRD STUDIES OF THE HYDRATION AND INTERLAYER STRUCTURE OF SMECTITES

In 1930, Hendricks and Fry (1930) were the first to present the crystalline nature of montmorillonite extracted from soil through the collection of an XRD pattern. The first crystal structure description was proposed soon after by Hofmann *et al.* (1933). These authors showed that few XRD bands were unaffected by dehydration. In contrast, one reflection was found to gradually migrate from 19.6 to 9.8 Å. Based on the structural description of kaolinite achieved just one year prior by Gruner (1932), Hofmann

https://doi.org/10.1346/CCMN.2016.0640401 Published online by Cambridge University Press

et al. (1933) concluded that the reflections that were not impacted by dehydration in montmorillonite could be assigned to hk0 bands, whereas intercalation of liquid water between the 2:1 layers was responsible for the migration of the 001 reflection related to a uniaxial swelling/shrinkage process.

In agreement with such a description, the successive works of Nagelschmidt (1936) and Maegdefrau and Hofmann (1937) also considered a smectite hydration process for smectite as the sorption of *n* water molecules. This structural description was, however, significantly improved by Bradley *et al.* (1937), who investigated the hydration of a Na^+-saturated montmorillonite through the gradual migration of the 001 reflection from 9.6 to 21.4 Å. These authors reported, however, that the hydration process only slightly impacted the XRD band located near 3 Å. Accordingly, these authors concluded that the hydration process occurred in montmorillonite in a stepwise manner, following the incorporation of *n* water planes. The intercalation of these water planes, each formed by 6 H_2O molecules per unit cell, was attributed to the presence of discrete and well defined hydration states at 9.6, 12.4, 15.4, 18.4, and 21.4 Å. Despite this novel description, Bradley *et al.* (1937) noted that the crystal structure was more complex than previously thought. Bradley's remark was related to the absence of two respective 001 reflections at the transition between two hydration states; instead, a significant broadening of the 001 reflection was observed.

Soon after the description of interlayer water organization in terms of water planes, the work of Hendricks and Jefferson (1938) rationalized the different previous studies into a single and consistent structural model for montmorillonite. These authors first noticed that the interlayer model of Bradley *et al.* (1937) was similar to that of Gruner (1934) obtained for vermiculite. This latter author reported that the structure of vermiculite was distinct from that of hydrobiotites or chlorites, with the presence of 8 H_2O molecules per unit cell forming two planes of water molecules (4 H_2O per plane). On this basis, Hendricks and Jefferson (1938) proposed that montmorillonite and vermiculite could both be considered as swelling clay minerals, with interlayer water forming a flat hexagonal network (Figure 2). These authors reported that the high number of H_2O molecules per plane of water (*i.e.* 6 *vs.* 4 H_2O per unit cell for Bradley *et al.*, 1937, and Hendricks and Jefferson, 1938, respectively) in montmorillonite was likely related to water sorption on the external surfaces of the minute-sized smectite particles. Finally, Hendricks and Jefferson (1938) discussed the antagonism between the gradual hydration process described by several authors (Hofmann *et al.*, 1933; Nagelschmidt, 1936; Maegdefrau and Hofmann, 1937) based on the gradual shift of the 001 reflection and the sequential stepwise hydration mechanism originally proposed by Bradley *et al.* (1937). Hendricks and Jefferson (1938) proposed that in the specific case of a crystal that contains layers with different numbers of water planes, the resulting 00*l* XRD reflections would present a narrow reflection at 3 Å and a broader 001 reflection that could be only described as intermediate with an apparent *d*-spacing between those expected for homogeneous structures. Such a short description reconciled the different studies that had been performed until that time and paved the way for further studies on the diffraction of mixed-layer clay minerals (Hendricks and Teller, 1942; Méring, 1949; among others).

Interestingly, although the foundations of the interlayer water organization and hydration process in montmorillonite were laid in 1938, the exact positions of cations compensating the layer charge of the 2:1 layers were still debated. Soon after the description of the first structural model of montmorillonite by Hofmann *et al.* (1933), Hofmann and Bilke (1936) and later Gieseking (1939) proposed that the compensating cations in montmorillonite were located on the edges of the particles. In contrast, other authors, such as Marshall (1935) for montmorillonite and Gruner (1934) for vermiculite, proposed a preferential location for cations in the interlayer space of swelling clay minerals. To resolve this question, Hendricks *et al.* (1940) combined thermal analysis and XRD for montmorillonite saturated with different cations. These authors showed that the dehydration temperature was dependent on the cationic nature and that such dehydration was systematically accompanied by a change in the 001 reflection position. This confirmed the presence of cations in the interlayer space of montmorillonite while further indicating a similar structural model for montmorillonite and vermi-

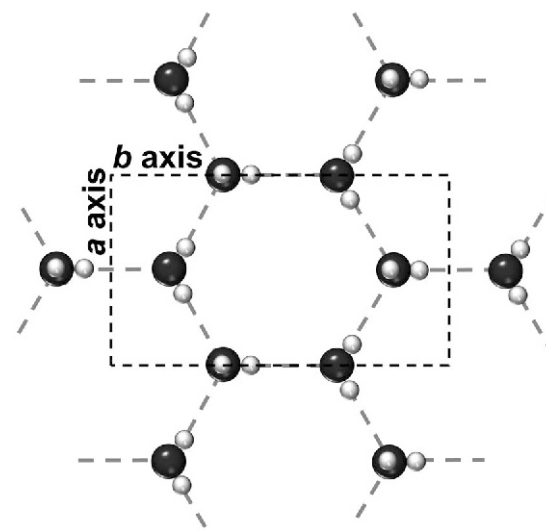

Figure 2. Pioneer model of interlayer water plane organization in a flat hexagonal network as proposed by Hendricks and Jefferson (1938).

https://doi.org/10.1346/CCMN.2016.0640401 Published online by Cambridge University Press

culite. Moreover, Hendricks *et al.* (1940) proposed that the interlayer hydration process was likely initiated by the hydration of the interlayer cation, followed by the sorption of additional water molecules for the completion of the hexagonal water network. Accordingly, Hendricks *et al.* (1940) were the first to invoke the presence of different types of water molecules in the interlayer space of swelling clay minerals.

The study of Hendricks *et al.* (1940) paved the way for a complete description of the heterogeneous and multi-scale nature of the hydration process in smectite, as was later proposed by Méring (1946) and remains current (Figure 3). Méring (1946) indeed proposed that montmorillonite hydration started by the hydration of the external surface of smectite particles that had formed by the juxtaposition of individual clay layers. This was followed by the hydration of the interlayer cations and then by filling the interlayer space with water molecules based on the hydration heterogeneities, *i.e.* the coexistence of layers with different hydration states in the same crystal was partly attributed by this author to the irregular distribution of charges among the layers. At a larger length scale and higher relative humidity, the water uptake was also accompanied by water absorption in the inter-particle porosity through a capillary condensation process (Figure 3; Méring, 1946).

In line with these previous works, many studies have focused on the homogeneous *vs.* heterogeneous nature of the hydration state in smectite as a function of the relative humidity and temperature (Glaeser and Méring, 1954, 1968; Méring and Glaeser, 1954; Pezerat and Méring, 1958; Pezerat, 1967; Glaeser *et al.*, 1967; Sato *et al.*, 1992, 1996; among others). These studies were mainly performed through the analysis of XRD 00*l* reflections due to the extreme disorder in the stacking sequence of smectite layers. Note, however, that the studies of Ben Brahim *et al.* (1983, 1984), based on analysis of hk*l* reflections, investigated the three-dimensional organization of water molecules and cations in the interlayer space of montmorillonite and beidellite as well as the layer stacking modes. Additional works on trioctahedral swelling clay minerals (*e.g.* vermiculite and saponite) have also shown an intimate relationship between the interlayer cation, the cation hydration shell, and the layer stacking mode (see the reviews by Suquet and Pezerat, 1987; de la Calle and Suquet, 1988).

The analysis of smectite hydration heterogeneity also benefited from theoretical developments in the consideration of structural defects, such as the influence of interstratification effects on the measured XRD peak intensity and position (*e.g.* see Reynolds, 1989; Drits and Tchoubar, 1990; Moore and Reynolds 1997; Sakharov and Lanson, 2013, for a more detailed description of the XRD profile calculation for defect structures). This led to the development of quantitative calculation routines devoted to the analysis of XRD basal reflection profiles, such as NEWMOD (Reynolds, 1967, 1985), ASN (Sakharov and Drits, 1973; Sakharov *et al.*, 1982a, 1982b), BGMN (Bergmann and Kleeberg, 1998; Ufer *et al.*, 2012), or, more recently, Sybilla (Aplin *et al.*, 2006), among others. The development of these routines allowed for the modeling of experimental XRD basal reflections that in turn provided quantitative insights into the nature, composition, and amount of different layer types which coexist in the smectite structure, as well as the mean crystal size in the direction normal to the layers. For instance, Moore and Hower (1986) showed that dehydrated and monohydrated layers could coexist in an ordered stacking sequence in Wyoming montmorillonite. For the same smectite, Cases *et al.* (1992, 1997) and Bérend *et al.* (1995) showed that three different types of layers could coexist in the same sample. Other quantitative studies on hydration heterogeneities in smectite have focused on the influence of many parameters, *i.e.*, the influence of cation nature (Cases *et al.* 1992, 1997; Bérend *et al.*, 1995; Cuadros, 1997; Ferrage *et al.*, 2005a, 2005b, 2007a; Dazas *et al.*, 2014), temperature (Ferrage *et al.*, 2007b), heteroionic interlayer chemistry (Iwasaki and Watanabe, 1988; Ferrage *et al.*, 2005c; Tertre *et al.* 2011b; Lanson *et al.*, 2015), relative humidity (Cases *et al.* 1992, 1997; Bérend *et al.*, 1995; Ferrage *et al.*, 2005a, 2007a, 2010; Dazas *et al.*, 2013, 2015), layer crystal chemistry (Calarge *et al.*, 2003; Christidis and

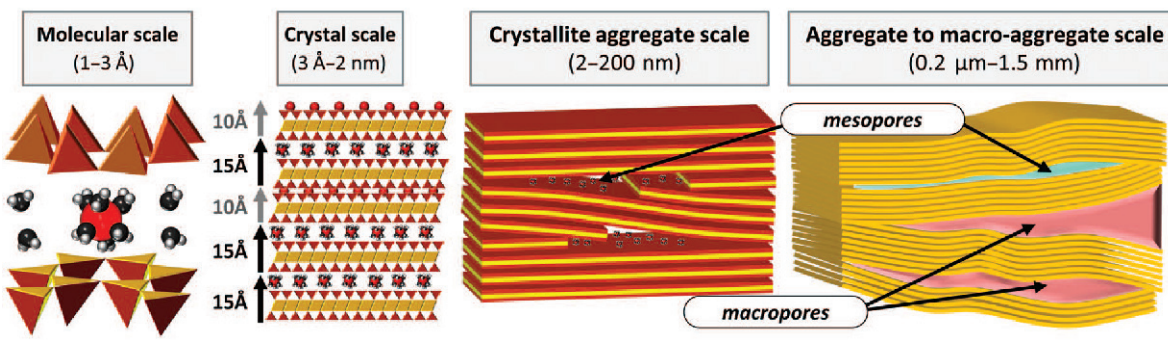

Figure 3. Schematized representation of the multi-scale organization of porous smectite media as proposed by Méring (1946).

https://doi.org/10.1346/CCMN.2016.0640401 Published online by Cambridge University Press

Table 1. Parameters for calculating X-ray atomic scattering factors (a_i, b_i, and c, from Waaszmaier and Kirfel, 1995) of neutral atoms and the bound coherent neutron scattering lengths (b_{coh}) of the most abundant isotopes for the different elements common in 2:1 clay minerals.

Element	a_1	a_2	a_3	a_4	a_5	c	b_1	b_2	b_3	b_4	b_5	b_{coh}
H	0.413048	0.294953	0.187491	0.080701	0.023736	0.000049	15.569946	32.398468	5.711404	61.889874	1.334118	−3.7406
D	–	–	–	–	–	–	–	–	–	–	–	6.6710
Li	0.974637	0.158472	0.811855	0.262416	0.790108	0.002542	4.334946	0.342451	97.102966	201.363831	1.409234	−2.2200
C	2.657506	1.078079	1.490909	−4.241070	0.713791	4.297983	14.780758	0.776775	42.086842	−0.000294	0.239535	6.6511
O	2.960427	2.508818	0.637853	0.722838	1.142756	0.027014	14.182259	5.936858	0.112726	34.958481	0.390240	5.8030
F	3.511943	2.772244	0.678385	0.915159	1.089261	0.032557	10.687859	4.380466	0.093982	27.255203	0.313066	5.6540
Na	4.910127	3.081783	1.262067	1.098938	0.560991	0.079712	3.281434	9.119178	0.102763	132.013947	0.405878	3.6300
Mg	4.708971	1.194814	1.558157	1.170413	3.239403	0.126842	4.875207	108.506081	0.111516	48.292408	1.928171	5.6600
Al	4.730796	2.313951	1.541980	1.117564	3.154754	0.139509	3.628931	43.051167	0.095960	108.932388	1.555918	3.4490
Si	5.275329	3.191038	1.511514	1.356849	2.519114	0.145073	2.631338	33.730728	0.081119	86.288643	1.170087	4.1070
K	8.163991	7.146945	1.070140	0.877316	1.486434	0.253614	12.816323	0.808945	210.327011	39.597652	0.052821	3.7400
Ca	8.593655	1.477324	1.436254	1.182839	7.113258	0.196255	10.460644	0.041891	81.390381	169.847839	0.688098	4.8000
Ti	9.818524	1.522646	1.703101	1.768774	7.082555	0.102473	8.001879	0.029763	39.885422	120.157997	0.532405	−6.0800
Cr	11.007069	1.555477	2.985293	1.347855	7.034779	0.06551	6.366281	0.023987	23.244839	105.774498	0.429369	4.9200
Mn	11.709542	1.733414	2.673141	2.023368	7.003180	−0.147293	5.597120	0.0178	21.788420	89.517914	0.383054	−3.7300
Fe	12.311098	1.876623	3.066177	2.070451	6.975185	−0.304931	5.009415	0.014461	18.743040	82.767876	0.346506	9.9400
Co	12.91451	2.481908	3.466894	2.106351	6.960892	−0.936572	4.507138	0.009126	16.438129	76.98732	0.314418	2.4900
Ni	13.521865	6.947285	3.866028	2.1359	4.284731	−2.762697	4.077277	0.286763	14.622634	71.96608	0.004437	10.3000
Cu	14.014192	4.784577	5.056806	1.457971	6.932996	−3.254477	3.73828	0.003744	13.034982	72.554794	0.265666	7.7180
Zn	14.741002	6.907748	4.642337	2.191766	38.424042	−36.915829	3.388232	0.243315	11.903689	63.31213	0.000397	5.6800
Rb	8.123134	2.138042	6.761702	1.156051	17.679546	1.139548	15.142385	33.542667	0.129372	224.132507	1.713368	7.0300
Sr	17.730219	9.795867	6.099763	2.620025	0.600053	1.140251	1.563060	14.310868	0.120574	135.771317	0.120574	7.1500
Cs	17.418674	8.314444	10.323193	1.383834	19.876251	−2.322802	0.399828	0.016872	25.605827	233.339676	3.826915	5.4200
Ba	19.747343	17.368477	10.465718	2.592602	11.003653	−5.183497	3.481823	0.371224	21.226641	173.834274	0.010719	4.8400

Eberl, 2003; Ferrage *et al.*, 2007a, 2010; Dazas *et al.*, 2013, 2015), and compaction (Holmboe *et al.*, 2012) on the proportion and composition of the different hydrates.

THEORETICAL BASIS FOR CALCULATING THE 00*l* REFLECTIONS IN SMECTITE XRD PATTERNS

The quantitative studies mentioned above performed using XRD modeling of basal reflection positions and profiles all demonstrated that hydration heterogeneity is the rule for smectite. Irrespective of the XRD analysis conditions or the sample considered, few smectites consist of 100% of one type of layer. Moreover, these studies confirmed the previous interpretation regarding the restricted range of layer-to-layer distances for the different hydrates (Figure 1) even though the first reflection could gradually migrate on the experimental pattern. This heterogeneous nature of the smectite structure has noticeable implications for the design of molecular simulations. These simulations are indeed most often performed considering a periodic structure, *i.e.* a structure composed of layers having the same layer-to-layer distance (or d_{001} value). The structural significance of the obtained experimental distance is, however, complicated in the case where the smectite structure exhibits hydration heterogeneity and/or thin crystal sizes.

In this section, the different steps for calculating a theoretical diffraction pattern with 00*l* reflections to compare with an experimental XRD diffractogram are detailed for a periodic smectite structure using conventional spreadsheet software. This simplified theoretical description was envisioned with three main objectives in mind. First, the description of homogeneous hydration states shown below allows XRD pattern 00*l* reflections to be calculated using conventional spreadsheet software and simplified descriptions of interlayer models. Thus, the calculations can be used for educational purposes to assess the sensitivity of XRD 00*l* reflection intensities for a wide range of interlayer compositions and organizations. Second, the theoretical background will be used in the next section to describe how different parameters (hydration heterogeneity, crystallite size effects) can complicate the extraction of true d_{001} values and potential ways to overcome this limitation. Third, the theoretical background detailed below provides information to calculate the theoretical pattern profile of 00*l* reflections from simulations for comparison with experimental XRD data in order to validate interlayer molecular models.

Basics for calculating an XRD pattern 00l reflections for a homogeneous smectite structure

In the following, different parameters for calculating the 00*l* reflections for an approximate XRD pattern for a periodic and homogeneous structure are described from the scattering of individual atoms to the diffraction produced by a powder with many crystals (Figure 3) in order to allow comparisons between diffraction and molecular simulation results. For further details on calculating the diffracted intensity of defect clay structures, the reader should refer to the existing literature (Reynolds, 1989; Drits and Tchoubar, 1990; Moore and Reynolds, 1997; Sakharov and Lanson, 2013).

Atomic scattering factor. At the atomic scale, the interaction of X-rays with electrons is described through the atomic scattering factor, f_n, which is the scattering amplitude of X-rays by an isolated atom n. This factor accounts for the amount of scattering and distances between scattering centers (electrons in this case) and can be expressed as a function of the diffraction angle (θ) and X-ray wavelength (λ) according to (Waasmaier and Kirfel, 1995):

$$f_n^0(\theta) = c + \sum_{i=1}^{5} a_i \exp(-b_i \sin^2\theta/\lambda^2) \quad (1)$$

The a_i, b_i, and c parameters for different common atoms in clay minerals were obtained from Waazmaier and Kirfel (1995) and are reported in Table 1. For some of these atoms, calculation of the $f_n^0(\theta)$ function was performed using the $K\alpha_{1+2}$ wavelength of copper radiation $\lambda(CuK\alpha_{1+2})$ = 1.5418 Å (Figure 4a). Because of the interaction of X-rays with electrons, the function $f_n^0(\theta)$ is closely related to the number of electrons in the atom n, which implies that XRD will be extremely sensitive to heavy atoms, such as Fe in clays, and less sensitive to hydrogen (Figure 4a). Moreover, because the electrons are not located at the atom's nucleus, the scattering of X-rays by the atom is less efficient when the spatial length scale d is decreased, *i.e.* when θ ($\sin\theta = \lambda/2d$) is increased. Considering the interaction of neutrons with matter, scattering centers are located at atomic nuclei, and the atomic scattering factor of each atom n is then described through the bound coherent scattering length b_{coh} (Table 1, Figure 4b) of the atom. The b_{coh} is angle-independent but depends on the actual nucleus composition and will thus differ for different isotopes of the same element. The atomic scattering factors, calculated using Equation 1, are commonly corrected for thermal motion effects as in Equation 2 (Moore and Reynolds, 1997):

$$f_n(\theta) = f_n^0(\theta)\exp(-B_n\sin^2\theta/\lambda^2 \quad (2)$$

Where B_n is the Debye-Waller factor of the atom (in Å^2) and corresponds to the mean square displacement of an atom n from the ideal position in the structure.

Layer scattering factor. Because of the two-dimensional periodicity of clay layers, the layer scattered amplitude can be calculated based on the nature of atoms and the

https://doi.org/10.1346/CCMN.2016.0640401 Published online by Cambridge University Press

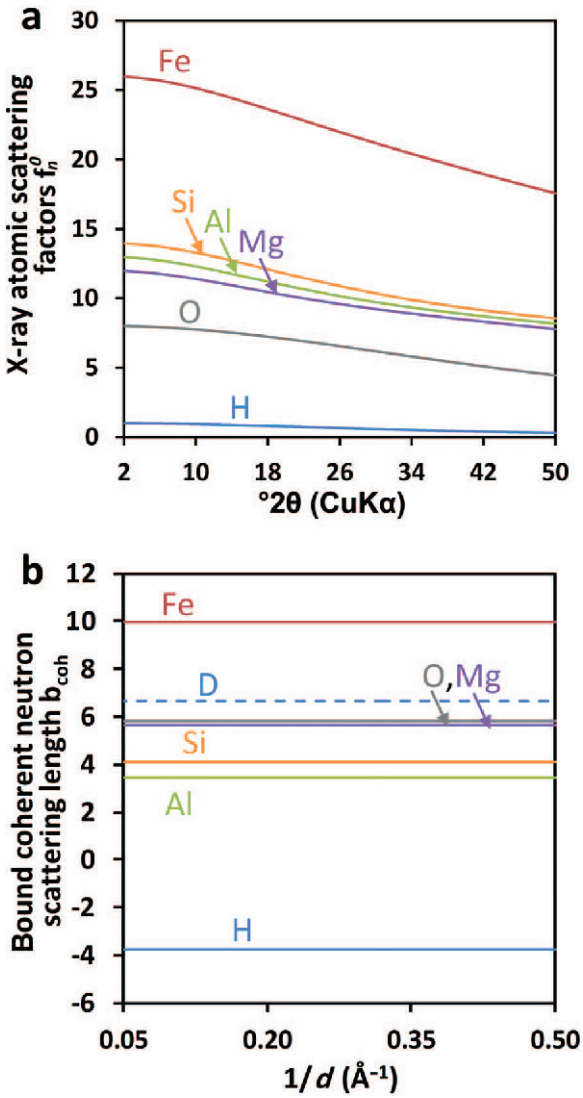

Figure 4. (a) Variation as a function of the diffracting angle θ of the atomic scattering factor for X-rays $f_n^0(\theta)$ for different common atoms in clay minerals (Equation 1) (with $\lambda(CuK\alpha_{1+2})$ = 1.5418 Å). (b) Variation for the corresponding $1/d$ values ($1/d = 2\sin\theta/\lambda$) of the bound coherent neutron scattering length b_{coh}.

coordinates along the c* direction of the unit cell (*i.e.* along the direction normal to the plane surface of the 2:1 layer). In centrosymmetric unit cells, used for smectite and vermiculite clay minerals, the layer scattering factor (G) can be described for basal reflections as a function of the diffraction angle θ as in Equation 3 (Moore and Reynolds, 1997):

$$G(\theta) = \sum_n P_n f_n(\theta) \cos(4\pi Z_n \sin\theta/\lambda) \qquad (3)$$

where $f_n^0(\theta)$ is the atomic scattering factor of atom n given by Equation 2, P_n is the quantity of atom n, and Z_n is the absolute Z-coordinate of atom n (in Å) in the unit cell. The Z_n, P_n, and B_n values for the montmorillonite 2:1 layer are considered here (Figure 5a). Interlayer structural models for dehydrated, mono-hydrated, bi-hydrated, and tri-hydrated layers (Figure 5), and selected ranges of values for the Z_n, P_n, and B_n parameters from the literature (Table 2) were also considered. The origin of the unit cell used to define the Z-coordinate for all atoms is located on the layer mirror plane in the center of the octahedral sheet. For the calculation of $G(\theta)$, only the half unit cell is sufficient, *i.e.* the values of Z, P, and B for atoms located between the cationic plane in the center of the octahedral sheet and the interlayer mid-plane located at $z = d_{001}/2$ (basal spacing d_{001} in Å; Figure 5a). The square of the function $G(\theta)$, which accounts for the relative intensities of the 00l reflections (see below), is calculated (Figure 6) for montmorillonite unit cells with 0 to 3 water planes. For these calculations, the Z_n, P_n, and B_n parameters for atoms constituting the 2:1 layer are considered (Figure 5a), and the parameters for the interlayer cations and water molecules, together with the d_{001} values associated with the different montmorillonite hydrates are reported in Table 3. The slope of the $[G(\theta)]^2$ function strongly decreased for 2θ angles <10° for all layer types and for 2θ >10° modulated the relative intensities of the 00l reflections in the final XRD pattern. As noted above, the term $\exp(-B_n\sin^2\theta/\lambda^2)$ in Equation 2 is introduced to account for the thermal fluctuation of atom n. When the angle θ is increased, the increase in B_n decreases the contribution of the atom to the scattered intensity. Different B_n values can be attributed to the same type of atom in the smectite structure depending on the position (*e.g.* interlayer *vs.* 2:1 layer), which is typically the case for oxygen atoms. Contrasting B_n values are commonly assigned to oxygen atoms from the 2:1 layer or from the interlayer water molecules (Figure 5; Tables 2 and 3). High values (>10 Å) attributed to the B_n parameter do not have any significance in terms of thermal motion but rather describe the distribution along c* of the species, as detailed below.

Interference function. At a larger length scale, the intensity diffracted by a lamellar crystal depends on the distances between the individual layers along the direction normal to the surface of the clay layers. In a periodic structure, *i.e.* a crystal composed of M identical layers of basal spacing d_{001} (in Å), the so-called interference function is given by Moore and Reynolds (1997):

$$\phi(\theta) = \frac{1}{M}\frac{\sin^2(2\pi M d_{001}\sin\theta/\lambda)}{\sin^2(2\pi d_{001}\sin\theta/\lambda)} \qquad (4)$$

The function $\phi(\theta)$ (Figure 7a) displays 00l maxima at positions d_{001}/l. The coherent scattering domain (CSD) size, which corresponds to the product of the number of layers M and the basal spacing d_{001} value, affects the breadth of the reflection series. The ripples can be eliminated by considering a distribution of CSD sizes in

https://doi.org/10.1346/CCMN.2016.0640401 Published online by Cambridge University Press

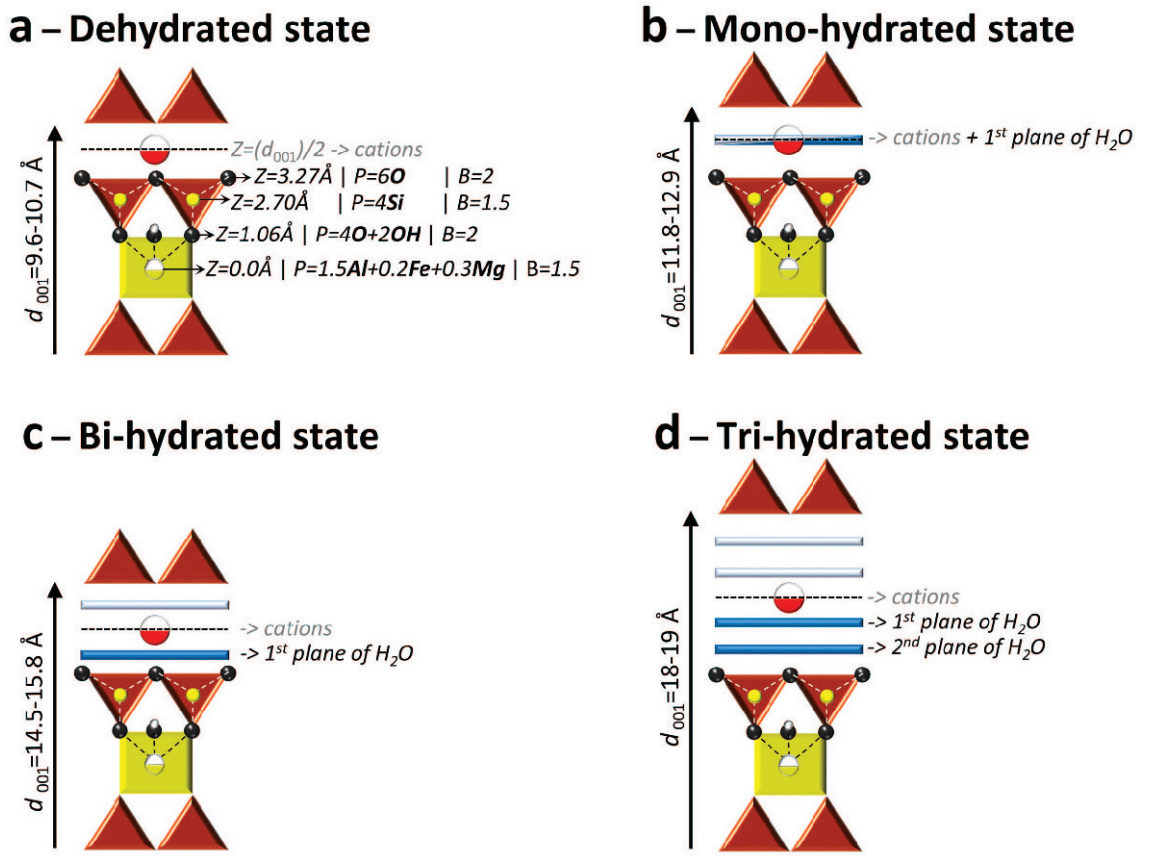

Figure 5. Schematized structural models of montmorillonite layers for (a) dehydrated state, (b) mono-hydrated state, (c) bi-hydrated state, and (d) tri-hydrated state. For each plane, *Z*, *P*, and *B* denote the Z-coordinate (in Å, with origin in the octahedral sheet center and for one half unit cell), atomic nature and amount (for one half unit cell), and the Debye-Waller parameter (in Å^2), respectively. Parameters describing the interlayer model of water and cations in the different smectite hydrates are reported in Table 2. Only half of the interlayer space is represented for each hydration state, *i.e.* atoms with *Z*-coordinates lower than that of the interlayer mid-plane.

the powder (Drits *et al.*, 1997a). For a lognormal distribution of coherent scattering domain sizes, the fraction $F(M)$ of crystals with a number M of layers can be calculated as (Drits *et al.*, 1997a):

$$F(M) = \frac{1}{\sqrt{2\pi}\beta M} \exp - \frac{(\ln(M) - \alpha)^2}{2\beta^2} \quad (5)$$

where the parameters α and β can be correlated to the mean number of layers, $\overline{M}$, of the distribution by α = 0.9485ln($\overline{M}$) − 0.017 and β = $\sqrt{}$(0.103ln($\overline{M}$) + 0.034), respectively (Drits *et al.*, 1997a). This distribution for three different $\overline{M}$ values (Figure 7b) is also defined by $\sum_{M=1}^{M_{max}} F(M) = 1$, with M as an integer (M = 1, 2, 3....) and $M_{max} = 5\overline{M}$ (for practical purposes, Sakharov and Lanson, 2013). By combining Equations 4 and 5, the interference function becomes:

$$\phi(\theta) = \sum_{M=1,2,3...}^{M_{max}} \frac{F(M)}{M} \frac{\sin^2(2\pi M d_{001} \sin\theta/\lambda)}{\sin^2(2\pi d_{001} \sin\theta/\lambda)} \quad (6)$$

The ripples are eliminated by applying this lognormal distribution (Figure 7c).

The last effect to be considered here for the calculation of the interference function is the fluctuation in layer-to-layer distance (*i.e.* in d_{001} value). This type of fluctuation was shown to be of two types (Guinier, 1964; Drits and Tchoubar, 1990; Sakharov and Lanson, 2013). In the first type, the fluctuations describe a distribution law, and the translation between two *n*th nearest-neighbor layers is equal to *n* times the average d_{001} value. For the second type of defect, this correlation between short- and long-range order is lost, and the total translation between two *n*th nearest-neighbor layers is no longer equal to *n* times the average translation. Both types of defect induce, however, a decrease in 00*l* intensities when increasing the diffraction angle. Although many studies have considered fluctuations of the second type (Sakharov and Lanson, 2013), the calculation using simple spreadsheet software for this second type of defect is not straightforward. For simplicity, let us thus consider fluctuations of the first

https://doi.org/10.1346/CCMN.2016.0640401 Published online by Cambridge University Press

Table 2. Range of values for layer-to-layer distance (d_{001}), Z-coordinate (Z_n, one half unit cell), amount (P_n, one half unit cell), and Debye-Waller (B_n) parameters from the literature to describe the interlayer structural models for the different smectite hydrates.

	Dehydrated state (0W)	Mono-hydrated state (1W)	Bi-hydrated state (2W)	Tri-hydrated state (3W)
d_{001}	9.6<x<10.7	11.8<x<12.9	14.5<x<15.8	18.0<x<19.5
Plane of interlayer cation				
Z_{cat}	$d_{001}/2$	$d_{001}/2$	$d_{001}/2$	$d_{001}/2-$[0<x<1.2]
P_{cat}	0.3 M^+	0.3 M^+	0.3 M^+	0.3 M^+
B_{cat}	2<x<10	2<x<10	2<x<10	20<x<45
1st plane of H_2O molecules				
$Z^1_{H_2O}$	–	$d_{001}/2$	$d_{001}/2-$[1.2<x<1.6]	$d_{001}/2-$[1.0<x<1.5]
$P^1_{H_2O}$	–	1<x<3	2<x<5	4<x<5
$B^1_{H_2O}$	–	2<x<30	2<x<40	~100
2nd plane of H_2O molecules				
$Z^2_{H_2O}$	–	–	–	$d_{001}/2-$[3.2<x<3.7]
$P^2_{H_2O}$	–	–	–	3.0<x<3.5
$B^2_{H_2O}$	–	–	–	10<x<15

The x stands for the accepted value for the parameter considered; Z_n and d_{001} are given in Å; For Z_n values, $d_{001}/2$ indicates the Z-coordinate of the interlayer mid-plane (see Figure 5); B_n values are given in Å^2; M^+ stands for the equivalent charge; The positions, amounts, and Debye-Waller parameters of atoms that constitute montmorillonite 2:1 layers are given in Figure 5a.

type, which lead to similar effects on the calculated profiles. By considering a normal distribution of average values of d_{001} and variance Δ (in Å, with $0 \leqslant \Delta < 1$ Å), defects of the first type in layer-to-layer fluctuations can be calculated by multiplying the interference function by the exponential term $\exp[-8(\pi\Delta\sin\theta/\lambda)^2]$ (Drits and Tchoubar, 1990; Sakharov and Lanson, 2013).

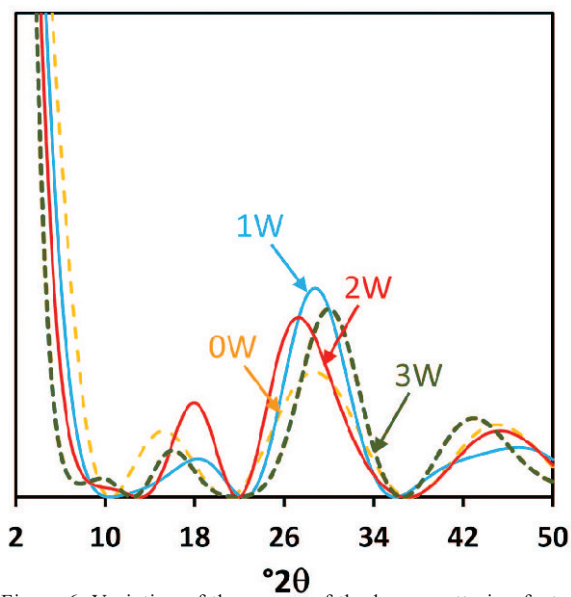

Figure 6. Variation of the square of the layer scattering factor $[G(\theta)]^2$ as a function of the diffracting angle θ calculated using Equation 3 for dehydrated (0W), mono-hydrated (1W), bi-hydrated (2W), and tri-hydrated (3W) layers.

The combination of both the distribution of CSD sizes and the fluctuation of the layer-to-layer distance leads to the following expression of the interference function:

$$\phi(\theta) = \sum_{M=1,2,3\ldots}^{M_{max}} \frac{F(M)}{M} \frac{\sin^2(2\pi M d_{001}\sin\theta/\lambda)}{\sin^2(2\pi d_{001}\sin\theta/\lambda)} \exp[-8(\pi\Delta\sin\theta/\lambda)^2] \quad (7)$$

An increase in the Δ parameter from 0 to 0.5 Å (Figure 7d) decreases the intensity when the angle θ is increased.

Lorentz-polarization factor. The intensity of X-rays scattered by the sample must be corrected for different effects that are related to the nature and geometry of the interaction (Drits and Tchoubar, 1990; Moore and Reynolds, 1997; Sakharov and Lanson, 2013). Among the effects, changes in the sample volume that is actually diffracting with changes in angle θ and the polarization effects of X-rays after interaction with the sample is described (for X-ray diffractometers operating in reflection geometry with one or two Soller slits) through the Lorentz-polarization function as (Reynolds, 1986):

$$Lp(\theta) = \frac{(1+\cos^2 2\theta)\Psi}{\sin\theta} \quad (8)$$

https://doi.org/10.1346/CCMN.2016.0640401 Published online by Cambridge University Press

Table 3. Fit parameters and interlayer water and cation organization used for calculating the layer scattering factors (Figure 6) and XRD profiles of 00*l* reflections (Figure 9).

	Dehydrated state (0W)	Mono-hydrated state (1W)	Bi-hydrated state (2W)	Tri-hydrated state (3W)
d_{001}	9.58	12.29	15.66	19.17
$\bar{M}$	8.8	9.0	9.0	8.5
Δ	0.55	0.78	0.83	0.90
k	1.0	0.9	0.7	0.4
Plane of interlayer cation				
Cation nature	Na	Li	Sr	Mg
Z_{cat}	$d_{001}/2$	$d_{001}/2$	$d_{001}/2$	$d_{001}/2$
P_{cat}	0.3	0.3	0.15	0.15
B_{cat}	5	5	10	40
1st plane of H_2O molecules				
$Z^1_{H_2O}$	–	$d_{001}/2$	$d_{001}/2-1.56$	$d_{001}/2-1.30$
$P^1_{H_2O}$	–	2.6	3.5	5.0
$B^1_{H_2O}$	–	10	20	104
2nd plane of H_2O molecules				
$Z^2_{H_2O}$	–	–	–	$d_{001}/2-3.60$
$P^2_{H_2O}$	–	–	–	3.2
$B^2_{H_2O}$	–	–	–	12

Z_n, d_{001}, and Δ are given in Å. For Z_n values (for one half unit cell), the term $d_{001}/2$ indicates the Z-coordinate of the interlayer mid-plane (see Figure 5). B_n and $\bar{M}$ are given in Å^2 and in number of layers, respectively. Atomic content P_n values are given for one half unit cell. The Z-coordinates, amounts and B_n values for atoms constitutive of the 2:1 layer were taken from the dioctahedral model of Moore and Reynolds (1997) and are reported for montmorillonite elsewhere (Figure 5a).

In this expression, the parameter Ψ accounts for the partial orientation of crystals in the powder and for geometric properties of the diffractometer used (Reynolds, 1986). The trigonometric term is the Lorentz-polarization function, which accounts for changes of the diffracting sample volume with angle θ and the polarization effects. Irrespective of the degree of crystal orientation in the powder, the Lorentz-polarization function strongly decreases when θ is increased, especially in the $2\theta < 10^o$ angular region (Figure 8). A complete description of the calculation of Ψ is given by Reynolds (1986). For simplicity, one may consider $\Psi = 1/\sin^k\theta$, where the k value ranges between 1 and 0 for randomly and perfectly oriented powders, respectively (Moore and Reynolds, 1997).

Comparison with experimental data. By combining Equations 3, 7, and 8, the total diffracted intensity $I(\theta)$ can be calculated as a function of θ by the product

$$I(\theta) = [G(\theta)]^2\phi(\theta)Lp(\theta) \quad (9)$$

Experimental XRD patterns (Figure 9) are compared to theoretical XRD profiles calculated using Equation 9 for selected montmorillonite samples at different hydration states. The theoretical XRD patterns for 00*l* reflections (Figure 9) were calculated using Microsoft® Excel in the $2-50^o2\theta$ angular range with a step size of $0.04^o2\theta$ [$\lambda(CuK\alpha_{1+2}) = 1.5418$ Å]. Three worksheets are sufficient for these calculations:

- The first worksheet is dedicated to the tabulation of $f_n^0(\theta)$ on the basis of a_i, b_i, and c parameters (Table 1) for the different atoms or molecules that constitute the crystal structure using Equation 1. The scattering factor is also calculated for H_2O molecules and OH groups ($f^0_{H_2O}(\theta)$ and $f^0_{OH}(\theta)$, respectively) as the sum of the scattering factors from the constituent atoms [*e.g.* $f^0_{H_2O}(\theta) = 2f^0_H(\theta) + f^0_O(\theta)$]. The same worksheet is also used to calculate the temperature-corrected atomic scattering factors according to Equation 2. Finally, this worksheet includes calculation of the layer scattering function $G(\theta)$ (Equation 3) based on (i) the absolute atomic Z-coordinates Z_n (in Å), (ii) the amount of atom P_n, and (iii) the Debye-Waller parameter (in Å^2) for the constituent atoms of the montmorillonite 2:1 layer (Figure 5a), interlayer water, and cations (Table 3). The d_{001} values used to calculate the interlayer Z-coordinates are also reported (Table 3).
- The second worksheet is used to calculate a series of interference functions $\phi(\theta)$ for M = 1, 2, 3, M_{max} according to Equation 4 (M_{max} = 50 layers is enough for all calculations shown below). Each $\phi(\theta)$ function is then weighted by the $F(M)$ coefficient that is calculated based on the mean layer $\overline{M}$ number of the lognormal distribution (Equation 5). The sum of the series corresponding to Equation 6 that is obtained is

https://doi.org/10.1346/CCMN.2016.0640401 Published online by Cambridge University Press

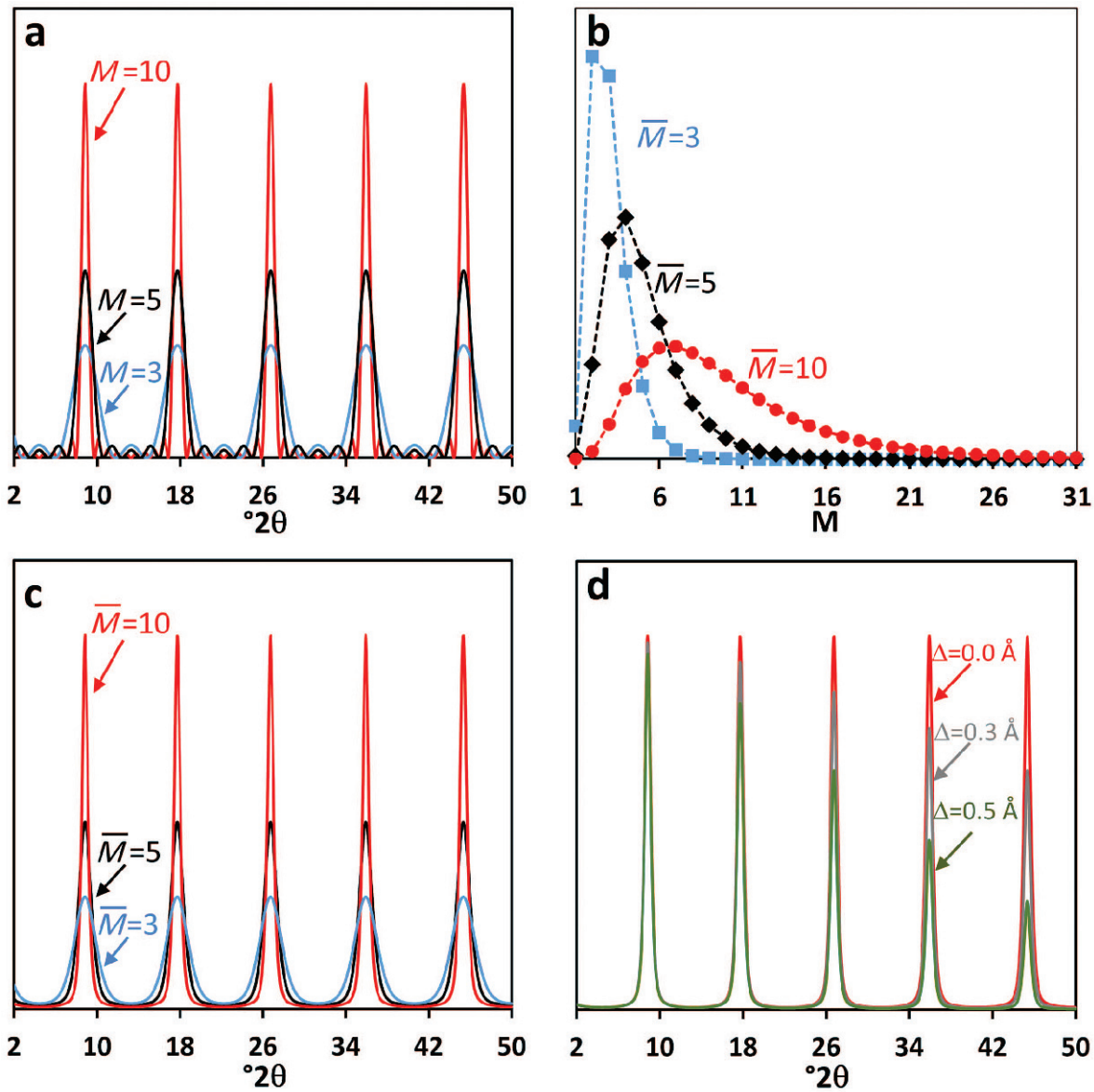

Figure 7. Variation as a function of diffracting angle θ of (a) the interference function ϕ(θ) for 00*l* reflections and crystals with a number of layers, $M = 10$, 5, or 3 (Equation 4, with $d_{001} = 10$ Å); (b) Shape of the $F(M)$ distribution of the number of layers in crystals with mean values of $\bar{M} = 10$, 5, or 3 (Equation 5); (c) Variation as a function of the diffracting angle θ of the interference function with the lognormal distributions of the layers in the crystals shown in (b) using Equation 6; (d) Influence of the fluctuation in layer thickness Δ parameter on the interference function (Equation 7 with $d_{001} = 10$ Å and $\bar{M} = 10$).

then multiplied by the exponential term $\exp[-8(\pi\Delta\sin\theta/\lambda)^2]$ (with the variance parameter Δ of the normal distribution in Å, Table 3) to account for fluctuation of the first type in layer-to-layer distances and obtain the full interference function ϕ(θ), as reported in Equation 7.

- The third and last worksheet is used to calculate the Lorentz-polarization function (*i.e.* $Lp(\theta)$ using k values, Table 3). On the same worksheet, the product of $Lp(\theta)$ and the full ϕ(θ) function (Equation 7) and the square of the layer scattering function $G(\theta)$ (*i.e.* $[G(\theta)]^2$) is calculated to obtain the $I(\theta)$ intensities according to Equation 9. The intensities of the calculated pattern obtained for 00*l* reflections is then normalized on the 001 reflection intensity and then compared to the experimental pattern which is also normalized in the same manner.

For 0, 1, and 2W hydration states, the experimental patterns obtained for oriented preparations of <1 μm SWy-1 were used (Ferrage *et al.*, 2005a). The nature of the interlayer cation (Na, Li, and Sr, respectively) and the relative humidity (secondary vacuum, 60%, and

https://doi.org/10.1346/CCMN.2016.0640401 Published online by Cambridge University Press

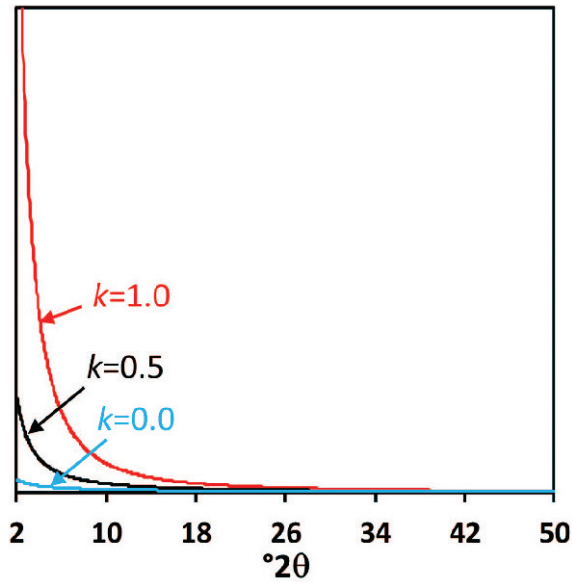

Figure 8. Variation of the Lorentz-polarization factor $Lp(\theta)$ as a function of the diffracting angle θ using Equation 8 and different values for the k parameter.

80%, respectively) were chosen to limit hydration heterogeneity, thus leading to the presence of 93% or more of a given layer type for all samples. For the 3W hydration state, the experimental pattern obtained by Dazas *et al.* (2014) for Mg-saturated, <2 μm SWy-2 equilibrated at 99% relative humidity was considered because the sample contained 98% 3W layers under these conditions (Dazas *et al.*, 2014).

Although hydration heterogeneities were not considered, the simplified theoretical description above can be used to satisfactorily fit (Figure 9) all measurable 00*l* reflections in the $2 < 2\theta < 50°$ angular region for quasi-homogeneous hydration states. The structure model and fit parameters used to reproduce the experimental data (Figure 9) included d_{001}, $\overline{M}$, Δ, and k, as well as the Z_n, P_n, and B_n values for the different planes of water molecules or cations (Table 3). Other parameters, such as the Z_n, P_n, and B_n values for montmorillonite 2:1 layer atoms (Figure 5a), were used without further adjustments. With regard to the content, position, and distribution of water molecules, the obtained values are similar to those derived by Ferrage *et al.* (2005a, 2005b) for 0-2W and by Dazas *et al.* (2014) for the 3W hydration state despite the simplified approach used in the present study. Note, however, the misfit in the low-angle region for most samples. This misfit is related to an incorrect description of inter-crystalline defects, as discussed by Sakharov and Lanson (2013), which does not impact the relative intensities of the 00*l* reflections. A good quality of fit, discarding this low-angle region misfit, is obtained when the unweighted Rp parameter reaches values of <7%, with this parameter being defined as (Howard and Preston, 1989).

$$Rp = \sqrt{\frac{\sum[I_{\text{exp}}(2\theta_i) - I_{\text{calc}}(2\theta_i)]^2}{\sum I_{\text{exp}}(2\theta_i)^2}} \quad (10)$$

One should emphasize that the simplified calculation formalism considered here is restricted to a single and unique periodic smectite structure composed of >90% of one type of hydrate. Moreover, due to the significant approximations considered in this formalism and because different parameters have similar effects on the calculated 00*l* intensities, no physical interpretation should be given to parameters related to particle orientation (k values) or fluctuations in layer-to-layer distance (Δ values).

METHODOLOGY FOR THE COMBINED USE OF DIFFRACTION EXPERIMENTS AND MOLECULAR SIMULATIONS

As detailed above, the XRD technique is particularly effective for the experimental determination of the layer-to-layer distance d_{001} value (through the interference function $\phi(\theta)$) and of the composition and organization of the smectite structure (through the layer scattering function $G(\theta)$). Calculation of the theoretical pattern of 00*l* reflections for a periodic smectite structure (Figure 9) is also approachable as an assessment of basic interlayer organization (Figure 5, Table 3).

In the following section, the methodology of combining diffraction, experiments, and molecular modeling data using a back-and-forth procedure is detailed. In the first part of this section, emphasis is placed on the limitations of XRD for the refinement of interlayer disorder in water and ion organization. These limitations can be overcome using molecular simulations, which likely provide more realistic 3D descriptions of the three-dimensional organization of water and ions in smectite. These molecular simulations are most often performed by considering a periodic structure, *i.e.* a structure composed of layers having the same d_{001} value. This value is, however, commonly derived from the angular position of the first low-angle peak on the XRD pattern and the transformation to the layer-to-layer distance using Bragg's law ($2d_{001}\sin = \lambda$). The structural significance of the obtained distance is subject to bias when the smectite structure exhibits hydration heterogeneity and/or thin crystal size. The second part of this section focuses on the extraction of the "true" d_{001} value to design a molecular simulation for the investigation of interlayer organization in smectite. Finally, the third part of this section presents how the Z-distributions of interlayer species (water, ions, and other compounds) derived from molecular simulations can be incorporated into the calculation of a theoretical 00*l* profile for comparison with experimental data using conventional spreadsheet software. Such a comparison is advantageous for the validation of molecular models because

https://doi.org/10.1346/CCMN.2016.0640401 Published online by Cambridge University Press

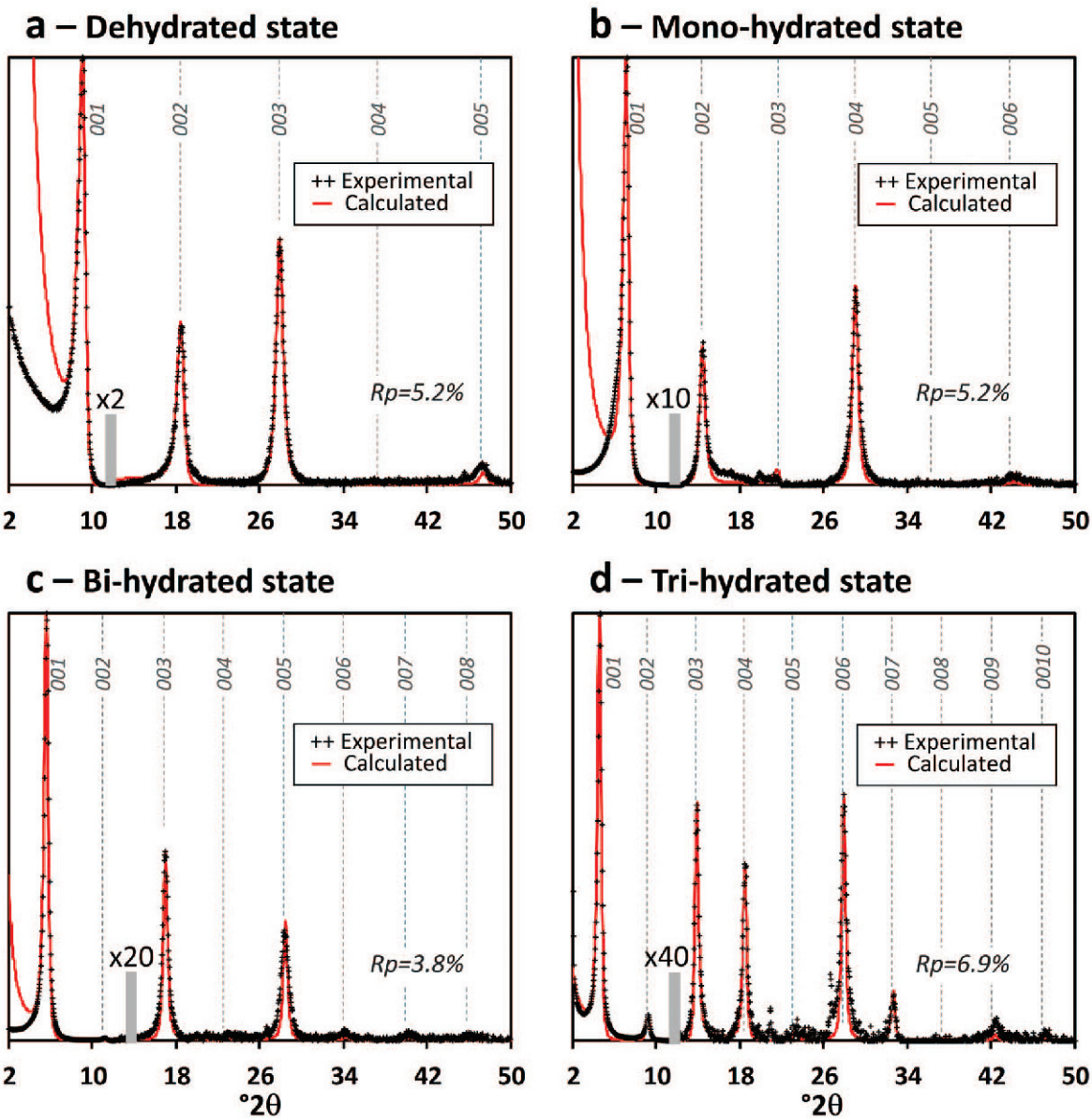

Figure 9. Comparison between experimental XRD patterns (crosses) and theoretical profiles (solid lines) of 00*l* reflections calculated using Equation 9 for different hydration states in montmorillonite; (a) dehydrated state of Na-saturated SWy-1 montmorillonite, (b) mono-hydrated state of Li-saturated SWy-1 montmorillonite, (c) bi-hydrated state of Sr-saturated SWy-1 montmorillonite, and (d) tri-hydrated state of Mg-saturated SWy-2 montmorillonite. The experimental data of (a–c) were adapted from Ferrage *et al.* (2005a), whereas the experimental pattern of (d) was adapted from Dazas *et al.* (2014). The vertical gray bar indicates an increased intensity scale factor for high-angle reflections ($2\theta > 12°$). Vertical dashed gray lines indicate the theoretical position of the 00*l* reflections. The fit parameters and interlayer organization of water and cations used for the calculation are reported in Table 3. Misfits between experimental and theoretical XRD patterns in the low-angle region were not considered in calculating the goodness-of-fit *Rp* parameter.

diffraction methods and molecular modeling probe the clay material at a similar length scale. Methods such as MD or MC strongly depend on the set of partial atomic charge and Lennard-Jones (LJ) parameters assigned to the clay and interlayer atoms and used to evaluate Coulombic and van der Waals interactions, respectively. Thus, extensive comparison with experimental data is necessary to assess the validity of the theoretical models (Striolo, 2011).

Limitations of XRD for the investigation of interlayer organization in smectite

The calculation of theoretical XRD patterns, as performed above based on a simplified structural

https://doi.org/10.1346/CCMN.2016.0640401 Published online by Cambridge University Press

model (Figure 5, Table 3), presents two major drawbacks for the refinement of the interlayer organization of water and cations in smectite. First, as X-rays interact with electrons, the diffracted intensity is solely sensitive to the distribution of electrons along the c*-axis in the structure, irrespective of the nature of the atoms. This strongly complicates assigning the electronic content between the different species that coexist in the structure (*e.g.* electrons from interlayer water molecules *vs.* electrons from interlayer cations). Moreover, the contributions of different atoms to the diffracted intensity differ as a function of both of the nature and amounts as well as the type of radiation used (X-ray or neutron; Figure 10). As an illustration, the relative contribution of atom n to the diffracted intensity was calculated as $P_n f_n^0(\theta = 0)$ for a high-charge [1.4 per $O_{20}(OH)_4$] bi-hydrated saponite sample (Figure 10a). As expected, XRD is not very sensitive to hydrogen atoms either from interlayer water molecules or from the 2:1 layer (Figure 10a). Similarly, the limited contribution of interlayer Na^+ cations indicates that XRD is not very sensitive to the Na^+ position, even for high-charge smectite. Second, according to the description of interlayer organization (Figure 5, Table 3), interlayer species in the different smectite hydrates are considered to lie on a limited number of discrete planes to reduce the number of variable parameters, that leads to a simplified and likely simplistic representation of the organization of interlayer species, which is similar to the hexagonal network organization of water molecules (Figure 2) and was originally evoked in the study of Hendricks and Jefferson (1938).

Few improvements of the interlayer models have been possible, however, based on modeling experimental 00*l* reflection series. Ferrage *et al.* (2005a) showed (Figure 11a) that the original interlayer model for bi-hydrated smectite proposed by Moore and Reynolds (1997) did not correctly account for the distribution of intensities on the experimental XRD profile, even if only high-intensity reflections with d >3.0 Å were considered. By replacing the original model of Moore and Reynolds (1997) that contained three sets of planes of water molecules in the interlayer with a single set of planes with a low Debye-Waller value (B_n = 2 Å^2), the fit was significantly improved despite several remaining misfits for low-intensity high-order 00*l* reflections (Figure 11b). To improve the comparison with experimental patterns, the same authors later proposed an interlayer water model in which the water molecules are distributed around a single set of Z-positions according to a Gaussian distribution (Figure 11c; Ferrage *et al.*, 2005b). The positional distribution of water molecules (or cations) as a Gaussian distribution characterized by full width at half-maximum (FWHM) values has the same influence on the calculated diffracted intensity as the thermal fluctuation effects accounted for by the Debye-Waller value through the following relation

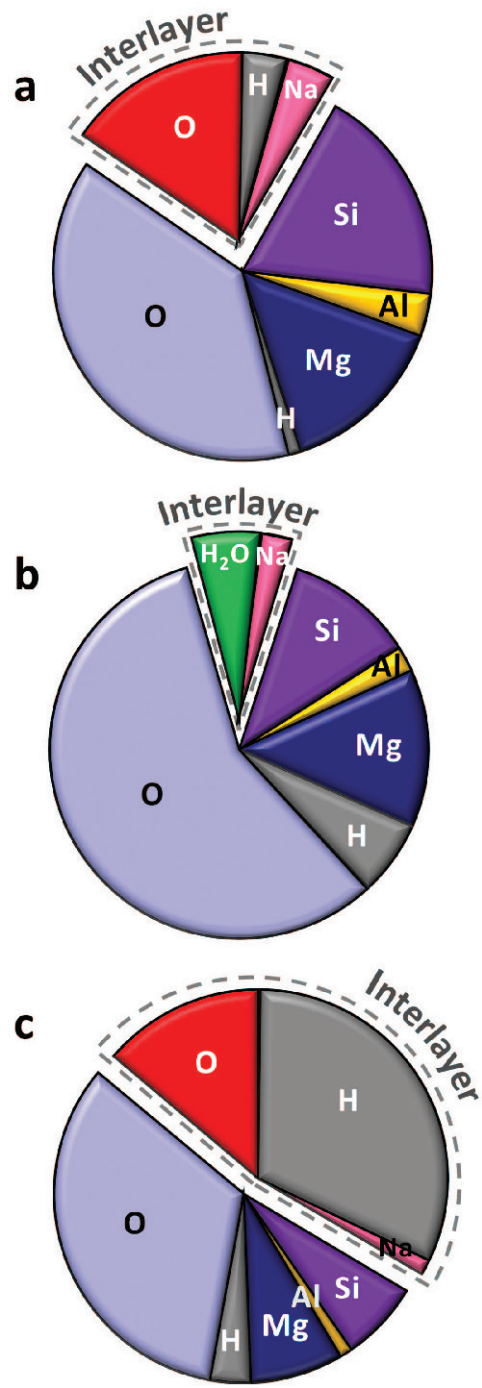

Figure 10. Relative contributions of the different atoms to the structure factor for the three diffraction methods (adapted from Ferrage *et al.*, 2011a). Calculations performed for a bi-hydrated and Na-saturated high-charge [1.4 charge per $O_{20}(OH)_4$] saponite with 10 H_2O molecules per unit cell; (a) X-rays for neutral atoms and with atomic scattering factors (Equation 1) considered at θ = 0; (b) neutrons on hydrogenated samples (taking into account the partial cancellation of interlayer water contribution, see text for details); (c) neutrons on deuterated samples.

https://doi.org/10.1346/CCMN.2016.0640401 Published online by Cambridge University Press

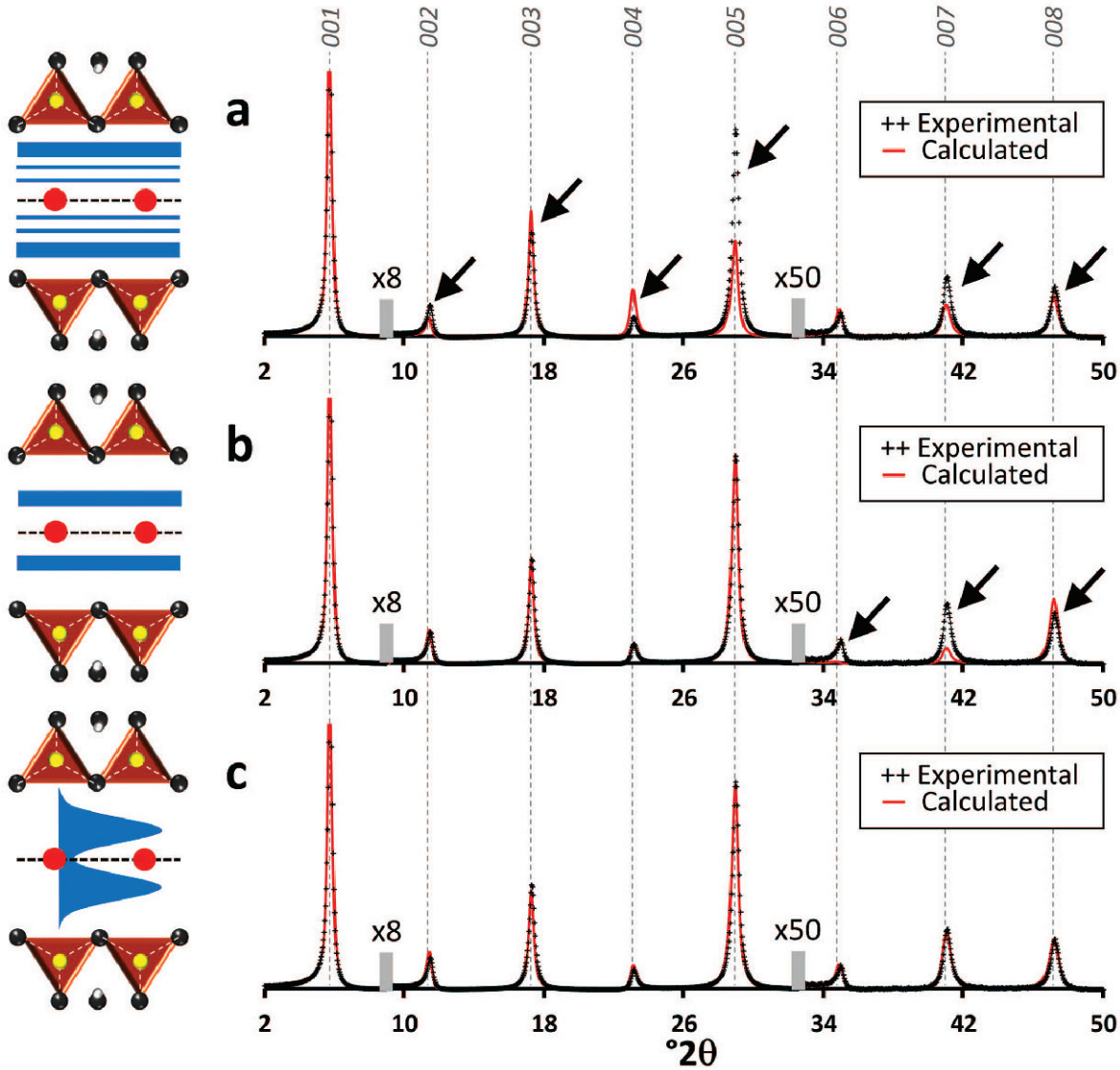

Figure 11. Comparison between different interlayer models of water and cations for a bi-hydrated and Na-saturated low-charge (0.8 charge per $O_{20}(OH)_4$) saponite sample recorded at 90% relative humidity; (a) interlayer model of Moore and Reynolds (1997); (b) interlayer model of Ferrage *et al.* (2005a); (c) interlayer model of Ferrage *et al.* (2005b). Left: Schematic representation of interlayer water and cations for the different interlayer models. Right: Comparison between experimental (crosses) and calculated profiles (solid line, adapted from Ferrage *et al.*, 2005b). Solid arrows indicate a significant misfit between the experimental and calculated patterns. The vertical gray bars indicate an increased intensity scale factor for high-angle reflections compared to the 001 reflection region.

(Shashikala *et al.*, 1993; Dazas *et al.*, 2013):

$$\mathrm{FWHM} = \frac{\sqrt{B_n}\sqrt{\ln(2)}}{\pi} \qquad (11)$$

Accordingly the quantity $P_n(z)$ of atom n distributed along Z can be described from the values of parameter B_n and coordinate Z_n as

$$P_n(z) = \frac{2\sqrt{\pi}}{\sqrt{B_n}} \exp\left[-\frac{4\pi^2(z - Z_n)^2}{B_n}\right] \qquad (12)$$

with $\Sigma P_n(z) = P_n$. The values >10 Å^2 assigned to parameter B_n for the water molecules (Figure 5; Tables 2 and 3) do not have any significance in terms of thermal motion but rather describe the positional disorder of interlayer water molecules (Ferrage *et al.*, 2005b; Dazas *et al.*, 2013, 2014, 2015).

https://doi.org/10.1346/CCMN.2016.0640401 Published online by Cambridge University Press

Such a water distribution about a "most probable" position is a step away from the hexagonal water network model (Figure 2) but still represents a rough approximation of the positional disorder of interlayer water molecules and cations commonly derived using molecular simulations. The structural studies on the organization of water and cations in smectite using XRD alone cannot answer questions regarding (i) the differentiation between water molecules coordinated (or not) to interlayer cations or (ii) the role played by the 2:1 layer crystal-chemistry on the orientation of water molecules. Although molecular simulations do not account for smectite hydration heterogeneity, these methods are perfectly suited to overcome the limitations of classical structural studies because of the ability to unravel the details in the organizational and dynamical properties of the fluid confined in the smectite interlayers.

Extraction of the layer-to-layer distance from experimental XRD pattern to be used in molecular simulations

The layer-to-layer distance d_{001} value is a key parameter to define the volume of the simulation box for molecular simulations of the smectite structure. This parameter is often derived from experimental XRD studies and, in particular, from the position of the 001 reflection. From a theoretical perspective, the positions of the 001 and other 00*l* reflections are related to the interference function. From the analysis of this function reported in Equation 4 for a homogeneous structure without hydration heterogeneity, the peaks are indeed located at the $d_{00l} = d_{001}/l$ positions. This latter relation indicates that the 00*l* reflection series is "rational," *i.e.* with $d_{001}/d_{00l} = l$. In practice, the 00*l* reflection series is, however, rarely rational in smectite, and as mentioned by Hendricks and Jefferson (1938), the position of the 001 reflection is then only apparent and does not correspond to the actual layer-to-layer distance in smectite to be used in molecular simulations. Here, the two effects that most often induce bias in the measurement of d_{001} values from experimental XRD patterns and some ways to overcome this difficulty will be described.

Effect of crystallite size. For a homogeneous smectite structure, an apparent shift of the 001 reflection from its theoretical position has been described as also resulting from the small crystallite size of smectite along the direction normal to the clay layers (Reynolds, 1968; Ross, 1968; Trunz, 1976; Drits and Tchoubar, 1990; Stanjek, 2002). For crystals composed of a low number of layers, *i.e.*, for $\overline{M} < 20$, as is most often the case in smectite, the resulting position of the 00*l* reflection series is affected by the slope of both the layer scattering and Lorentz-polarization factors (Figure 6). For a bi-hydrated Sr-saturated smectite structure calculated previously (Figure 9c), the decrease in the $\overline{M}$ value induces significant modifications on the calculated profiles (Figure 12a). These changes include a shift of the 001 and 005 reflections toward lower angles (*i.e.* higher *d* values) and a shift of the 003 reflection toward higher angles, leading to irrationality in the 00*l* reflections series. This effect is even more dramatic for the 001 reflection position and for structures with high hydration states because of the negative slope of both the layer scattering factor (Figure 6) and the Lorentz-polarization factor (Figure 8) in the $2\theta < 10^{\circ}$ angular region.

Effect of the interstratification of layers with different hydration states. The earlier studies on smectite demonstrated that smectite crystals most often exhibit interstratification of different hydrates. For a complete theoretical description of the XRD response from interstratified crystals, the reader should refer to existing books (Drits and Tchoubar, 1990; Moore and Reynolds, 1997; Sakharov and Lanson, 2013). For simplicity, consider the three extreme interstratification types (random, segregated, and ordered) for a Na-montmorillonite structure composed of mono-hydrated layers with d_{001} (1W) = 12.5 Å and bi-hydrated layers d_{001} (2W) = 15.0 Å in equal proportion ($W_{1W} = W_{2W} = 0.5$). The junction probability to find a 2W layer following a 2W layer is defined as P_{2W-2W}. This parameter is sufficient to calculate XRD patterns for random, segregated, and ordered mixed-layer structures in the specific case of short-range order factor R = 1 (Figure 12b; calculations performed using the ASN program; Sakharov *et al.*, 1982a, 1982b), according to Markovian statistics (Hendricks and Teller, 1942; Bethke and Altaner, 1986; among others). When $P_{2W-2W} = 1$, the layers are perfectly segregated in the structure, and the two rational series of 1W and 2W structures coexist on the resulting calculated pattern (Figure 12b). Thus, the XRD profile does not display a rational 00*l* series, in contrast to that obtained for a purely ordered structure with a maximum degree of ordering ($P_{2W-2W} = 0$). In this latter case, the crystals are composed of a perfect succession of 1W and 2W layers. This leads to a rational series of 00*l* reflections with a d_{001} value corresponding to the sum of d_{001} (2W) values (Figure 12b). The 001 reflection of this structure at ~27.5 Å is extremely weak in intensity compared with the 002 reflection at ~13.8 Å. When the layers are perfectly randomly distributed in the crystal ($P_{2W-2W} = W_{2W} = 0.5$), the obtained XRD pattern displays peaks in intermediate positions between those expected for periodic 1W or 2W structures. Moreover, the peak breadths of the resulting signal will depend on not only the mean coherent scattering domain size but also the angular distance between the positions expected for reflections of periodic 1W or 2W structures (Figure 12b). The influence of random interstratification on peak position, also known as Méring's rules (Méring, 1949), is responsible for the loss of rationality in the 00*l*

https://doi.org/10.1346/CCMN.2016.0640401 Published online by Cambridge University Press

reflection series. One should emphasize that for both random and perfectly ordered mixed-layer structures, the position of the most intense reflection at ~13.8 Å is only confusing because no layer in the stacking sequence displays such a layer-to-layer distance. Smectite crystal structures commonly exhibit a wide range of intermediate cases between homogeneous to random and/or partially segregated layer sequences. The partially ordered interstratification of layers with different hydration states appears, however, to be limited to low hydration states or to synthetic samples (Moore and Hower, 1986; Breu *et al.*, 2001; Ferrage *et al.*, 2010; Möller *et al.*, 2010; Dazas *et al.*, 2013).

Extraction of "true" layer-to-layer distances for the design of molecular simulations. As shown above, both layer interstratification (hydration heterogeneity) and thin crystallite size induce irrationality in 00*l* reflection series. This leads to an experimental XRD pattern with an apparent 001 position that differs from the actual layer-to-layer distance to be used in molecular simulations. As reported for Na-saturated montmorillonite as a function of relative humidity (Figure 12c), noticeable differences appear when comparing the "apparent d_{001}" derived from the 001 reflection position and the "mean thickness" of the layer obtained through the consideration of both hydration heterogeneity and thin crystallite size effects (Prêt *et al.*, 2013). The experimental 001 reflection tends to systematically overestimate the actual thicknesses of layers, a bias that can reach up to 20% of the actual interlayer volume at high relative humidity for this sample (Prêt *et al.*, 2013).

To improve the qualitative description of the experimental XRD pattern, a rationality estimate ξ parameter was proposed by Bailey (1982). This parameter can be used to assess the extent of heterogeneity in interstratified structures and is calculated as the standard

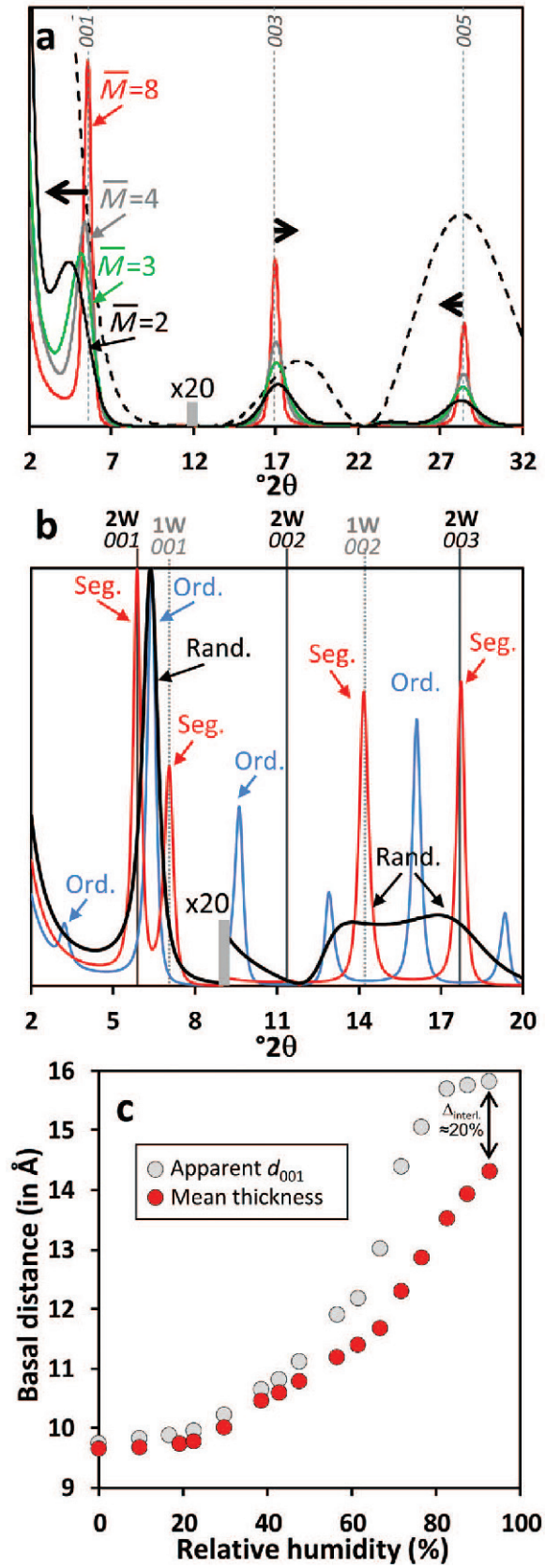

Figure 12. Effect of crystallite size and interstratification on the position of 00*l* reflections. (a) Influence of crystallite size on the position of 00*l* reflections. Calculation performed using Equation 9 for a bi-hydrated, Sr-saturated smectite (d_{001} = 15.66 Å, other parameters reported in Table 3) with mean numbers of layers of $\bar{M}$ = 8, 4, 3, and 2 in the structure. The dashed solid line reports the square of the layer scattering factor $[G(\theta)]^2$. (b) Calculated XRD pattern for a randomly interstratified (Rand., $P_{2W-2W} = W_{2W} = 0.5$), maximum degree of ordering (Ord., $P_{2W-2W} = 0$), and totally segregated (Seg., $P_{2W-2W} = 1$) mixed-layer structures composed of 2W and 1W layers in equal proportions. (c) Comparison between the apparent d_{001} value, measured through the position of the first diffraction maximum on the experimental XRD pattern, and the actual mean thickness of layers considering hydration heterogeneities (*i.e.*, relative proportions and respective layer-to-layer distances of the different types of layers). Data obtained for a Na-saturated montmorillonite as a function of relative humidity (adapted from Prêt *et al.*, 2013).

https://doi.org/10.1346/CCMN.2016.0640401 Published online by Cambridge University Press

deviation of $l \times d_{00l}$ values:

$$\xi = \sqrt{\frac{\sum_{i=1}^{n}\left[(l \times d_{00l})_i - \overline{l \times d_{00l}}\right]^2}{n-1}} \quad (13)$$

where $(l \times d_{00l})_i$ is the $l \times d_{00l}$ value for the i^{th} reflection (in Å) and $\overline{l \times d_{00l}}$ is the mean of the $l \times d_{00l}$ values calculated over a number of reflections n. As a general rule for smectite and irrespective of the hydration state, the structure can be considered quasi-homogeneous for $\xi < 0.1$ Å (measured for all 00l reflections in the $2 < 2\theta < 50°$ angular range; Ferrage *et al.*, 2005a, 2007a; Dazas *et al.*, 2014). Below 0.1 Å for the ξ parameter, the d_{001} value to be used to design molecular simulations can be obtained (i) from the average of $l \times d_{00l}$ values to reduce the contribution of crystal size effects ($\overline{d_{001}} = \overline{l \times d_{00l}}$) or (ii) using the theoretical formalism described above that implicitly considers CSD sizes. In the latter calculation, a simplified interlayer model (Figure 5) can be assumed to satisfactorily estimate the 00l positions (Figure 9). As an illustration, the calculation of the 00l reflections

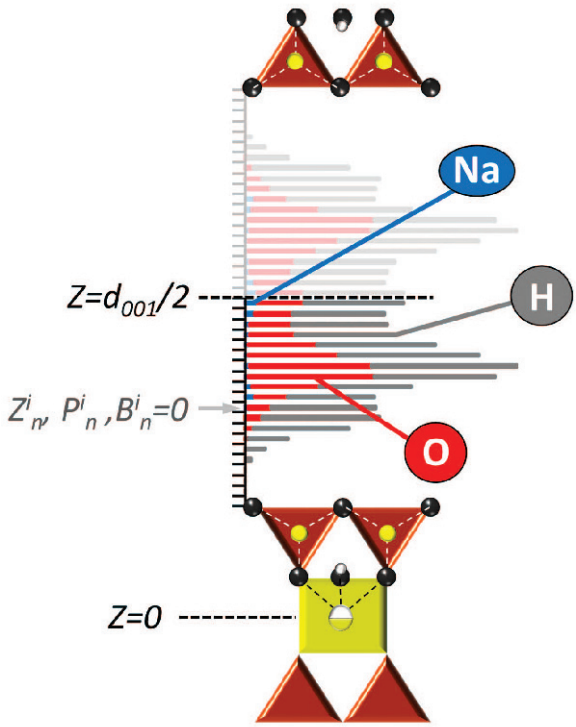

Figure 13. Methodology for generating XRD 00l reflections based on computed interlayer atomic density profiles derived from molecular simulations. Illustration shown for the atomic profile of Na, O, and H atoms for a Na-saturated, bi-hydrated, low-charge saponite sample (Ferrage *et al.*, 2011a). For each type n atom, the interlayer density profile is made symmetric with respect to the interlayer mid-plane and is separated into N individual atomic planes. Each plane i is characterized by the coordinate Z_n^i (origin in octahedral sheet center) and the quantity of atom P_n^i, with n = Na, O, or H, whereas the Debye-Waller B_n^i parameter is set to zero for all planes (see text for details).

diffraction profile of Sr-saturated montmorillonite in the bi-hydrated state (Figure 9c) was performed assuming a d_{001} value of 15.66 Å (Table 3), and the position of the first reflection on the pattern is at 15.75 Å (Figure 9c; Ferrage *et al.*, 2005a).

Generation of XRD profiles from computed atomic density profiles

Optimized Z-positions of interlayer cations and water molecules derived from molecular simulations can be validated by calculating theoretical diffraction patterns for comparison to experimental profiles. The methodology is shown for a Na-saturated and bi-hydrated saponite sample (Figure 13; Ferrage *et al.*, 2011a). The optimized position for interlayer Na, O, and H atoms, equilibrated in the μVT ensemble, is first made symmetric with respect to the mid-plane of the interlayer to respect the symmetry of the crystal. Then, the obtained profile is divided into N individual atomic planes (typically separated by a ΔZ of ~0.05 to 0.1 Å). Thus, each plane i is described by a coordinate Z^i (origin in the center of the octahedral sheet) and a quantity of atoms P_n^i, with n = Na, O, or H (Figure 13). Quantities of atoms P_n^i on each plane should be normalized to satisfy the relation $\sum_{i=1}^{N} P_n^i = P_n$. No thermal fluctuation parameter B_n is considered for these planes ($B_n^i = 0$) because the positional disorder related to temperature is commonly accounted for in the optimized atomic configurations extracted from molecular simulations. Finally, by considering only half of the interlayer space, *i.e.*, atoms with Z-coordinates lower than that of the interlayer mid-plane (Figure 13) as well as atoms constituting one half of the 2:1 layer (Figure 5a), the associated layer scattering factor and the overall theoretical XRD pattern for the 00l reflections can be calculated using Equations 3 and 9, respectively.

EXAMPLES OF AN IMPROVED DESCRIPTION OF THE INTERLAYER ORGANIZATION OF SMECTITE SPECIES FROM COMBINED USE OF EXPERIMENTAL AND NUMERICAL DATA

In the following section, recent advances in the investigation of interlayer water and ion organization in the different smectite hydrates (*i.e.* mono-, bi-, and tri-hydrated smectite) are presented. These examples are based on the back-and-forth procedure described above and provide key information on the local 3D interlayer organization of water and ions in smectite hydrates while validating the theoretical models through an extensive comparison with experimental diffraction data. This section also presents how this combined use of diffraction experiments and simulation results can be applied and easily transposed to other types of smectitic compounds, such as ethylene-glycol-montmorillonite complexes.

https://doi.org/10.1346/CCMN.2016.0640401 Published online by Cambridge University Press

Water and ion organization in mono- and bi-hydrated saponites

The combination of diffraction experiments and molecular simulations was applied to refine the interlayer organization of water and ions in two Na-saturated synthetic saponites with different layer charges [0.8 and 1.4 per $O_{20}(OH)_4$] and hydration states [mono- and bi-hydrated states] (Figure 14; Ferrage *et al.*, 2011a). Based on the layer-to-layer distance values obtained from the modeling of experimental XRD profiles (Ferrage *et al.*, 2010), Grand Canonical Monte Carlo (GCMC) simulations were performed assuming different clay and water models (Ferrage *et al.*, 2011a). The validity of the obtained GCMC results was assessed against different data sets. Water contents obtained from simulations were first compared to those obtained from water vapor desorption gravimetry experiments. Optimized positions of interlayer cations and water molecules were then introduced as initial parameters to generate 00*l* reflections either for X-ray or neutron diffraction (ND) patterns using the methodology shown above (Figure 13), and compared to experimental profiles (Figure 14). Neutron diffraction has a different sensitivity for atomic species in comparison to X-rays. Consequently, the contribution of an isolated atom *n* to the amplitude of neutron scattering ($f_n^0(\theta)$; Equation 2) is given by the bound coherent scattering length b_{coh}, which is independent of the angle θ (Figure 4b; Table 1), and provides greater intensity, high-order 00*l* reflections than X-rays. In addition, neutrons provide greater sensitivity than X-rays for light interlayer species, such as H atoms, and can be modified even further using deuterated water due to the different coherent scattering lengths of H and D atoms (Figure 4b, Table 1). Working on both hydrogenated and deuterated samples can impart

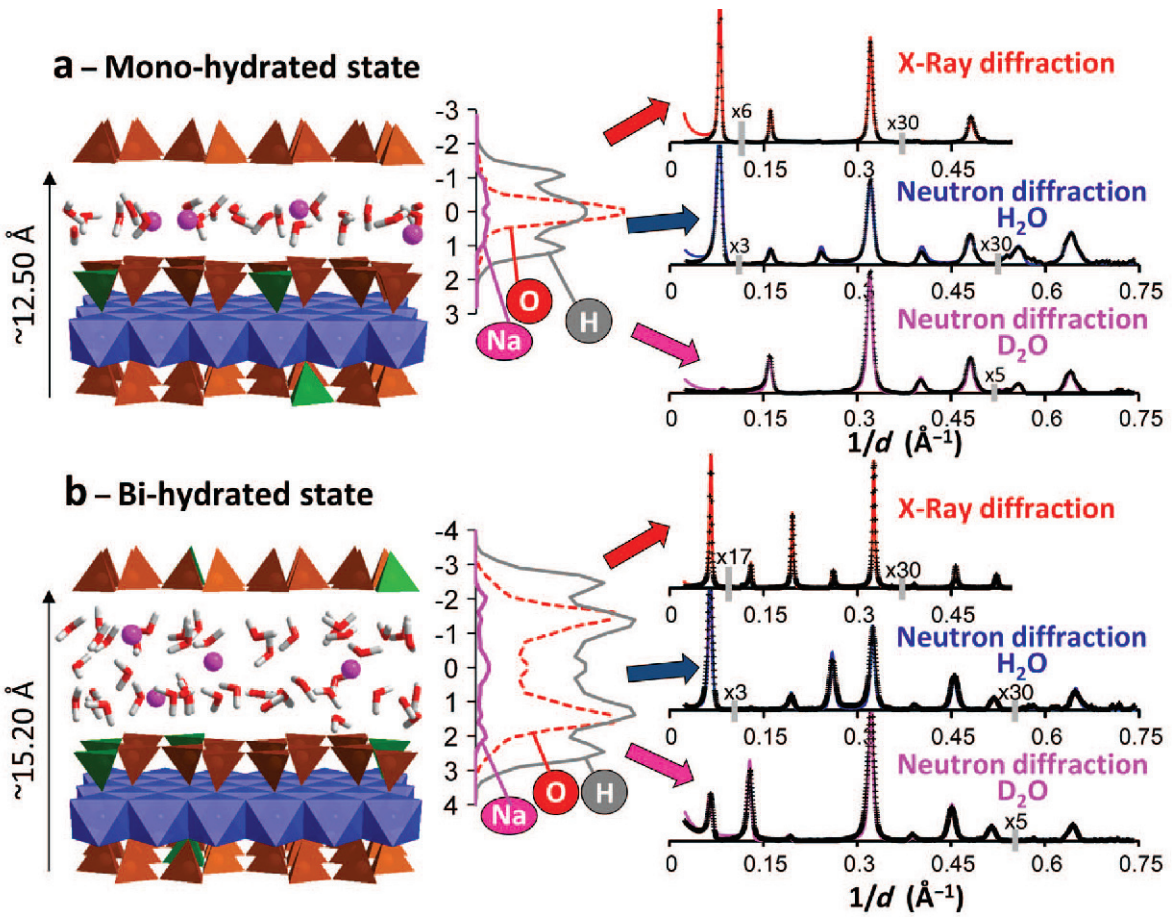

Figure 14. Refinement of water and ion organization in (a) mono- and (b) bi-hydrated Na-saturated saponite (adapted from Ferrage *et al.*, 2011a). Left: Snapshots of GCMC interlayer configurations for water and ions. Middle: Computed interlayer atomic density profile for sodium, oxygen, and hydrogen/deuterium atoms. Atomic *Z*-coordinates are given in Å relative to the interlayer mid-plane. Right: Experimental validation of computed interlayer organization through comparison of the experimental (crosses) and calculated (solid lines) X-ray diffraction and neutron diffraction 00*l* reflection profiles of both hydrogenated (H_2O) and deuterated (D_2O) saponite samples. The vertical gray bars indicate an increased intensity scale factor for the high-angle reflections compared to the 001 reflection region.

https://doi.org/10.1346/CCMN.2016.0640401 Published online by Cambridge University Press

additional constraints on the validation of the molecular simulation results (Figure 10; Martins *et al.*, 2014 and references therein). In the specific case of a hydrogenated specimen, the opposite signs of the bound coherent scattering lengths for oxygen (5.803 fm) and hydrogen (−3.7406 fm) can partially cancel the contribution of H_2O molecules to the diffracted intensity (Figure 10b). The H_2O molecules can indeed be considered as individual scatterers with a negligible coherent scattering length (−1.678 fm, Figure 10c) when the periodicities investigated in the crystal are larger than the O−H distance in water (1 Å). Under such conditions, neutron diffraction on a hydrogenated specimen provides additional constraints on the atomic positions in the 2:1 layer structure. The interlayer organization in saponites investigated following the methodology proposed by Ferrage *et al.* (2011a) showed that though not fully unequivocal, a proper fit of XRD patterns is an essential step in the validation of LJ parameters and atomic charges (Figure 14). Neutron diffraction on deuterated specimens clearly represented a step forward in this validation of clay and water models. This combination demonstrated that the CLAYFF model proposed by Cygan *et al.* (2004) described the content and organization of water more accurately than the models developed by Skipper *et al.* (1995) and Smith (1998). Once validated, analysis of the GCMC results deciphered the role played by layer charge in the orientation of interlayer water molecules (Ferrage *et al.*, 2011a) and in the distribution of interlayer cations within the *ab* plane (Dazas *et al.*, 2015).

Water and ion organization in tri-hydrated montmorillonite

Following a similar methodology, Dazas *et al.* (2014) recently refined the interlayer organization of water and ions in the interlayer space of tri-hydrated montmorillonite saturated with various cations (Mg, Ca, Ba, and Na; Dazas *et al.*, 2014). The experimental XRD patterns were first carefully analyzed to assess the rationality of the 00*l* reflection series. For all samples, the low values obtained for the rationality parameter ξ ($\xi \leqslant 0.06$ Å, Equation 13, Dazas *et al.*, 2014) allowed the layer-to-layer distances to be derived from the

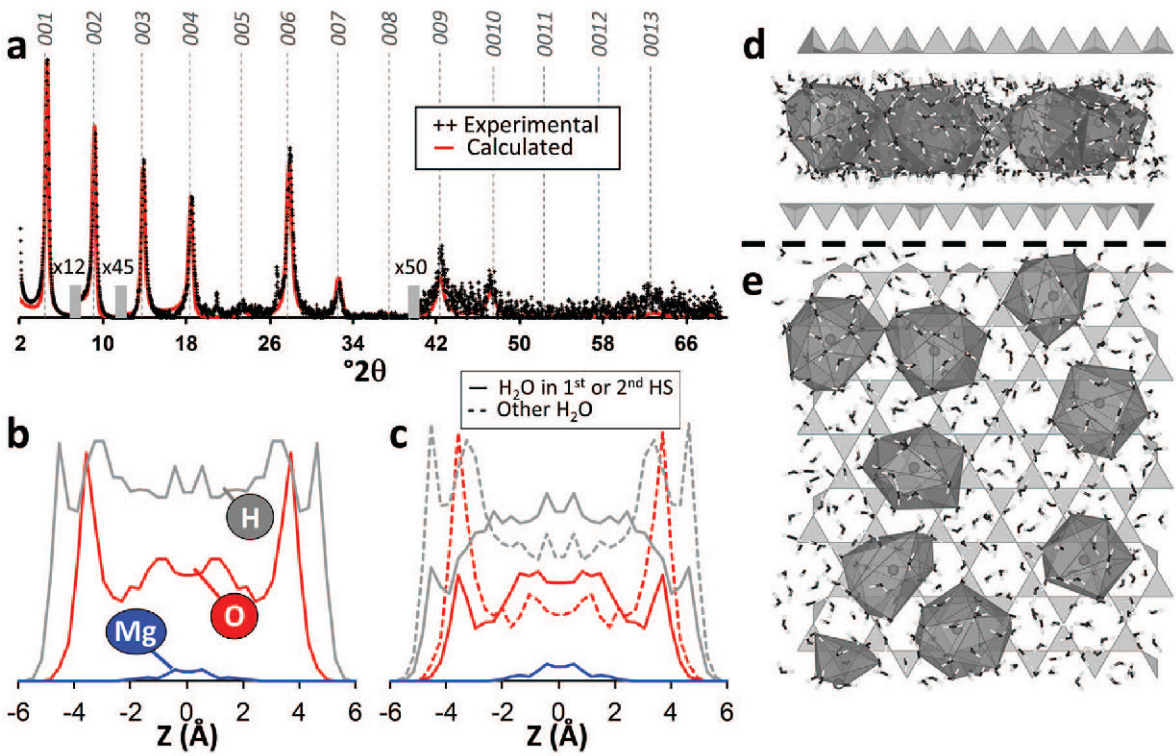

Figure 15. Refinement of water and ion organization in tri-hydrated, Mg-saturated montmorillonite (adapted from Dazas *et al.*, 2014). (a) Comparison of experimental (crosses) and calculated (solid line) XRD patterns. The vertical gray bars indicate an increased intensity scale factor for high-angle reflections compared to the 001 reflection region. The vertical dashed gray lines indicate the theoretical position of the 00*l* reflections. (b) Interlayer atomic density profile for Mg, O, and H atoms. Atomic *Z*-coordinates are given in Å relative to the interlayer mid-plane. (c) Discrimination between O and H atoms from water molecules contributing to the 1st and 2nd hydration shell (HS) of the interlayer cation (solid lines) and the same water molecule atoms filling the interlayer space (dashed line). (d) and (e) Snapshots of the GCMC configuration for water molecules from the second hydration shell of the cation projected along the *b*- and *c*-axes, respectively.

https://doi.org/10.1346/CCMN.2016.0640401 Published online by Cambridge University Press

average values of the $l \times d_{00l}$ products. After validating the GCMC results through comparing calculated and experimental XRD profiles (Figure 15a), the computed atomic density profiles were used to unravel the origin of the interlayer organization and stabilization of the trihydrated state. These authors showed that the atomic density profile did not correspond to the typical model of three discrete planes of H_2O molecules (Figure 1), but rather exhibited two sharp planes of H_2O molecules wetting the clay surfaces and additional poorly organized H_2O molecules filling the interlayer space (Figure 15b; Dazas *et al.*, 2014). Benefiting from the detailed interlayer picture provided by molecular simulations, the stability of the 3W hydrate was interpreted as resulting from the dual interactions of some H_2O molecules with interlayer cations through the second hydration shell and with the 2:1 layer surface (Figure 15c–e; Dazas *et al.*, 2014).

Water and ion organization in an ethylene-glycol-montmorillonite complex

The ethylene-glycol (EG) solvation of smectite interlayers is routinely used to assess the presence of expandable layers in polymineralic samples. Compared to air-dried (AD) preparations, the change in layer-to-layer distance and the presence of EG molecules in smectite interlayers indeed produce a significant change in the position and intensities of experimental 00*l* reflections. Both AD and EG treatments are also commonly applied to the same sample for the quantitative analysis of complex mixed-layer minerals using the XRD profile fitting method. According to the multi-specimen method proposed by Sakharov *et al.* (1999), a consistent structural model is obtained when the stacking sequences and proportions of the different layer types are nearly identical in both treatments. The fit of the EG-smectite experimental 00*l* reflections was performed using the interlayer EG model proposed by Reynolds (1965). According to this interlayer model, cations and water molecules are located on the same set of two planes, symmetrical with respect to the interlayer mid-plane, and located at +/−0.51 Å from the interlayer mid-plane. The summed quantities of water molecules plus cations on each plane are set at 1.2 per $O_{10}(OH)_2$ with a Debye-Waller factor of 2 Å^2. Two sets of two planes containing 1.7 CH_2OH groups with B_n = 11 Å^2 are used to describe the distribution of EG molecules in smectite interlayers. The interlayer atomic density profile $P_n(z)$ for the model of Reynolds (1965) can be calculated considering the thermal fluctuation in the atomic coordinate using Equation 12 (Figure 16a). Such a model has proven to be successful in the reproduction of 00*l* intensities for both pure smectite and mixed-layer structures containing smectite interlayers (Drits *et al.*, 1997b; Sakharov *et al.*, 1999; Lindgreen *et al.*, 2002; Claret *et al.*, 2004; Inoue *et al.*, 2005; Ferrage *et al.*, 2007a, 2011b; McCarty *et al.*, 2008, 2009; Lanson *et al.*, 2009; Hubert *et al.*, 2012; Viennet *et al.*, 2015; among others). Recently, Szczerba *et al.* (2014) reinvestigated the organization of cations, EG, and water molecules in the interlayer of Ca-saturated EG-solvated montmorillonite using MD simulations (Figure 16b). These authors showed that by using a more robust description of atomic interaction, as provided by MD simulations, the original mode of Reynolds (1965) could be reinterpreted. In particular, they were able to demonstrate that water molecules were spread along the c*-axis rather than forming two interlayer planes (Figure 16b).

Moreover, Szczerba *et al.* (2014) calculated the electronic density profile related to both models (Figure 16c). The latter is obtained by summing, for each plane i at a given Z-coordinate, the electronic content related to the amount and nature of atoms n lying on this plane as:

$$\rho^i = \sum_n P_n^i f_n^0(\theta = 0) \quad (14)$$

where the electronic density ρ^i is expressed in electrons. Szczerba *et al.* (2014) demonstrated that the two electronic maxima (Figure 16b) attributed by Reynolds (1965) to two sets of two planes that contain 1.7 $(CH_2OH)_2$ molecules were mostly due to the O and C atoms, respectively, from EG molecules (Figure 16c). Both models lead to similar electronic density profiles (Figure 16c), except near the interlayer mid-plane. For the model by Reynolds (1965), the interlayer distribution of water and molecules induces a sharp electronic profile in this region, whereas the interlayer mid-plane is depleted in electrons (Figure 16b). In contrast, the electronic density profile given by the model of Szczerba *et al.* (2014) is softer in the same region with noticeable electron density at the interlayer mid-plane. Because the electronic density profile of Reynolds (1965) has proven to be successful in reproducing 00*l* intensities, one may wish to assess whether the model proposed by Szczerba *et al.* (2014) can also produce a satisfactory fit of experimental XRD patterns. The experimental XRD patterns of Ca-saturated, EG-solvated, <1 μm SWy-1 montmorillonite was used for this test (Ferrage *et al.*, 2007a). Equation 9 and the strategy described above (Figure 13) were considered to generate the XRD 00*l* reflections. The fit parameters included the atomic positions and quantities of the montmorillonite 2:1 layer (Figure 5a) as well as d_{001} = 16.82 Å, $\overline{M}$ = 8.3 layers, Δ = 0.77 Å, and k = 0.6. A satisfactory fit of experimental data (Figure 16d) can be obtained using the model of Szczerba *et al.* (2014), thus providing an additional confirmation of the validity of this model.

CONCLUDING REMARKS AND PERSPECTIVES

The present article describes how a back-and-forth procedure between simulation results and diffraction data can improve the description of the smectite

https://doi.org/10.1346/CCMN.2016.0640401 Published online by Cambridge University Press

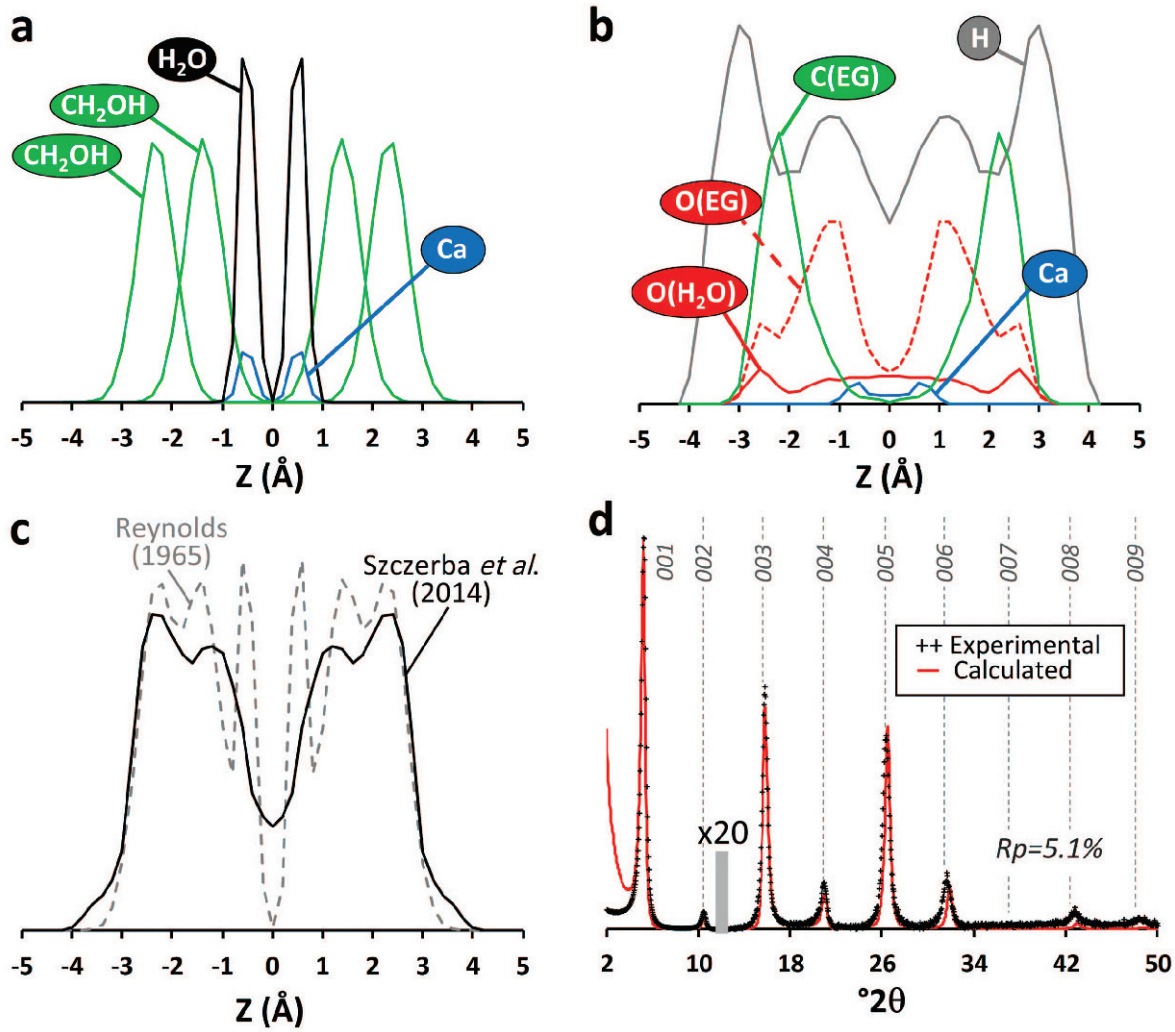

Figure 16. Refinement of the organization of water and ions in Ca-saturated ethylene-glycol/water-montmorillonite (adapted from Szczerba *et al.*, 2014); (a) Interlayer atomic density profile calculated according to the model of Reynolds (1965) and the distribution function along the c*-axis given by Equation 12. Atomic Z-coordinates are given in Å relative to the interlayer mid-plane. (b) MD-computed interlayer atomic density profile for Ca, O (from H_2O molecules), O (from EG molecules), C, and H atoms from Szczerba *et al.* (2014). (c) Comparison of the electronic density profiles ρ(*z*) obtained using the models of Reynolds (1965) and Szczerba *et al.* (2014). (d) Comparison of experimental XRD patterns (crosses) and theoretical profiles (solid lines) of the 00*l* reflections calculated using Equation 9 and the interlayer model of Szczerba *et al.* (2014) for Ca-saturated and EG-solvated SWy-1 montmorillonite (Ferrage *et al.*, 2007a). The vertical gray bar indicates an increased intensity scale factor for high-angle reflections (2θ > 12°). Vertical dashed gray lines indicate the theoretical position of the 00*l* reflections. Misfits between experimental and theoretical XRD patterns in the low-angle region were not considered in calculating the goodness-of-fit *Rp* parameter.

interlayer organization. The design of molecular simulations with layer-to-layer distances constrained by experimental diffraction data requires the biases related to hydration heterogeneities and thin crystallite sizes on the position of the first diffraction maxima to be considered. Based on molecular simulations results, computed interlayer positions can then be used to generate 00*l* reflection intensities for comparison with experimental diffraction data.

Results from molecular simulations strongly depend on the considered force field, which can still be improved, and thus, a comparison with experimental data is necessary for validation (Striolo, 2011). When interested in the interlayer organization of species, XRD data, in particular, are effective due to the similar length scale probed and the large accessibility of this diffraction technique. Thus, force field validation through comparison with XRD data is an essential step. Additional experimental data can, however, be necessary because of the aforementioned limitations of the XRD technique for the detection of light elements and interlayer cations. Once validated by comparison with experimental data, molecular simulations provide more realistic descriptions of the interlayer organization of

https://doi.org/10.1346/CCMN.2016.0640401 Published online by Cambridge University Press

water and ions in smectite. The obtained descriptions then supplement the structural refinements performed so far by (i) accessing the optimal interlayer position and realistic positional disorder for water and cations, and (ii) allowing for the examination of the structural properties of interlayer species in pressure and temperature conditions that are difficult to access experimentally. Moreover, with regard to water in smectite, the use of a force field validated by experimental data, such as CLAYFF, has also proven to be efficient in predicting dynamical properties of water molecules that are compatible with experimental neutron scattering data (Michot *et al.*, 2012; Martins *et al.*, 2014).

The collation of simulation results and diffraction data for the refinement of interlayer species organization is not restricted to the study of water and ions. As shown in the present paper, the methodology can be transferred to the analysis of ethylene glycol-montmorillonite systems. Thus, in principle, the same approach could provide additional experimental constraints on the ongoing development of force fields specifically designed to model organo-clay structures (Heinz *et al.*, 2005, 2013; among others). Organo-clay structures, such as intercalated smectite structures, commonly display a high degree of structural disorder in interlayer species, which preclude obtaining structural details using conventional diffraction experiments (Aristilde *et al.*, 2013). Moreover, a similar approach could be applied for the refinement of the interlayer organization of CO_2 in smectite (Fripiat *et al.*, 1974; Busch *et al.*, 2008; Botan *et al.*, 2010; Yang and Yang, 2011; Giesting *et al.*, 2012a, 2012b; Michels *et al.*, 2015). From a more general perspective, the back-and-forth procedure between experimental and numerical data proposed here could also be applied to other types of layered structures (*e.g.* layered oxides, carbons, layered double hydroxides). Similar to clay minerals, these lamellar structures commonly contain a high density of structural defects, and the intercalation properties have significant industrial or environmental implications (Lanson, 2011). In all cases, the simplified theoretical formalism for the calculation of 00*l* reflection series presented in this paper is likely applicable to a large number of lamellar host materials with a centrosymmetric crystal structure and a wide range of intercalated compounds. As a preliminary test, this formalism could be used to predict potential differences in experimental XRD responses among different types of interlayer models, either approached in a simplified manner (Figure 5) or as derived from molecular simulations performed using different force fields (Figure 13).

ACKNOWLEDGMENTS

Boris Sakharov is gratefully acknowledged for discussions of an earlier version of this manuscript regarding the theoretical aspects of XRD calculation. Constructive comments from Fabien Baron, Baptiste Dazas, Liva Dzene, Bruno Lanson, Alain Meunier, and Emmanuel Tertre also improved the manuscript. The CNRS interdisciplinary «défi Needs», through its «MiPor» program is thanked for the financial support provided for the present study (MPDYN project). The manuscript was much improved by the constructive comments of two anonymous reviewers and by the editorial suggestions of Acting Editor-in-Chief Michael Velbel.

REFERENCES

Akai, J., Nomura, N., Matsushita, S., Kudo, H., Fukuhara, H., Matsuoka, S., and Matsumoto, J. (2013) Mineralogical and geomicrobial examination of soil contamination by radioactive Cs due to 2011 Fukushima Daiichi nuclear power plant accident. *Physics and Chemistry of the Earth, Parts A/B/C*, **58–60**, 57–67.

Aplin, A.C., Matenaar, I.F., McCarty, D.K., and van der Pluijm, B.A. (2006) Influence of mechanical compaction and clay mineral diagenesis on the microfabric and pore-scale properties of deep-water Gulf of Mexico mudstones. *Clays and Clay Minerals*, **54**, 500–514.

Aristilde, L., Lanson, B., and Charlet, L. (2013) Interstratification patterns from the pH-dependent intercalation of a tetracycline antibiotic within montmorillonite layers. *Langmuir*, **29**, 4492–4501.

Bailey, S.W. (1982) Nomenclature for regular interstratifications. *American Mineralogist*, **67**, 394–398.

Ben Brahim, J.B., Armagan, N., Besson, G., and Tchoubar, C. (1983) X-ray diffraction studies on the arrangement of water molecules in a smectite. I. Homogeneous two-water-layer Na-beidellite. *Journal of Applied Crystallography*, **16**, 264–269.

Ben Brahim, J., Besson, G., and Tchoubar, C. (1984) Etude des profils des bandes de diffraction X dune beidellite-Na hydratée à deux couches deau. Détermination du mode dempilement des feuillets et des sites occupés par leau. *Journal of Applied Crystallography*, **17**, 179–188.

Bérend, I., Cases, J.M., François, M., Uriot, J.P., Michot, L.J., Masion, A., and Thomas, F. (1995) Mechanism of adsorption and desorption of water vapour by homoionic montmorillonites: 2. The Li^+, Na^+, K^+, Rb^+ and Cs^+ exchanged forms. *Clays and Clay Minerals*, **43**, 324–336.

Bergmann, J. and Kleeberg, R. (1998) Rietveld analysis of disordered layer silicates. Pp. 300-305 in: *Proceedings of the European Powder Diffraction* (*EPDIC5*) (R. Delhez and E.J. Mittemeijer, editors).

Bethke, C.M. and Altaner, S.P. (1986) Layer-by-layer mechanism of smectite illitization and application to a new rate law. *Clays and Clay Minerals*, **34**, 136–145.

Botan, A., Rotenberg, B., Marry, V., Turq, P., and Noetinger, B. (2010) Carbon dioxide in montmorillonite clay hydrates: Thermodynamics, structure, and transport from molecular simulation. *Journal of Physical Chemistry C*, **114**, 14962–14969.

Bradley, W.F., Grim, R.E., and Clark, G.F. (1937) A study of the behavior of montmorillonite upon wetting. *Zeitschrift für Kristallographie*, **97**, 216–222.

Breu, J., Seidl, W., Stoll, A.J., Lange, K.G., and Probst, T.U. (2001) Charge homogeneity in synthetic fluorohectorite. *Chemistry of Materials*, **13**, 4213–4220.

Brigatti, M.F., Galán, E., and Theng, B.K.G. (2006) Structure and mineralogy of clay minerals. Pp. 19–86 in: *Handbook of Clay Science* **1** (F. Bergaya, G.K.B. Theng, and G. Lagaly, editors). Developments in Clay Science, **1**. Elsevier, Amsterdam.

Busch, A., Alles, S., Gensterblum, Y., Prinz, D., Dewhurst, D., Raven, M., Stanjek, H., and Krooss, B. (2008) Carbon dioxide storage potential of shales. *International Journal of*

Greenhouse Gas Control, **2**, 297–308.

Calarge, L., Lanson, B., Meunier, A., and Formoso, M.L. (2003) The smectitic minerals in a bentonite deposit from Melo (Uruguay). *Clay Minerals*, **38**, 25–34.

Cases, J.M., Bérend, I., Besson, G., François, M., Uriot, J.P., Thomas, F., and Poirier, J.E. (1992) Mechanism of adsorption and desorption of water vapor by homoionic montmorillonite. 1. The sodium-exchanged form. *Langmuir*, **8**, 2730–2739.

Cases, J.M., Bérend, I., François, M., Uriot, J.P., Michot, L.J., and Thomas, F. (1997) Mechanism of adsorption and desorption of water vapor by homoionic montmorillonite: 3. The Mg^{2+}, Ca^{2+}, Sr^{2+} and Ba^{2+} exchanged forms. *Clays and Clay Minerals*, **45**, 8–22.

Christidis, G.E. and Eberl, D.D. (2003) Determination of layer-charge characteristics of smectites. *Clays and Clay Minerals*, **51**, 644–655.

Claret, F., Sakharov, B.A., Drits, V.A., Velde, B., Meunier, A., Griffault, L., and Lanson, B. (2004) Clay minerals in the Meuse-Haute Marne underground laboratory (France): Possible influence of organic matter on clay mineral evolution. *Clays and Clay Minerals*, **52**, 515–532.

Cuadros, J. (1997) Interlayer cation effects on the hydration state of smectite. *American Journal of Science*, **297**, 829–841.

Cygan, R.T., Liang, J., and Kalinichev, A.G. (2004) Molecular models of hydroxide, oxyhydroxide, and clay phases and the development of a general force field. *Journal of Physical Chemistry B*, **108**, 1255–1266.

Cygan, R.T., Greathouse, J.A., Heinz, H., and Kalinichev, A.G. (2009) Molecular models and simulations of layered materials. *Journal of Materials Chemistry*, **19**, 2470–2481.

Dazas, B., Lanson, B., Breu, J., Robert, J., Pelletier, M., and Ferrage, E. (2013) Smectite fluorination and its impact on interlayer water content and structure: A way to fine tune the hydrophilicity of clay surfaces? *Microporous and Mesoporous Materials*, **181**, 233–247.

Dazas, B., Ferrage, E., Delville, A., and Lanson, B. (2014) Interlayer structure model of tri-hydrated low-charge smectite by X-ray diffraction and Monte Carlo modeling in the grand canonical ensemble. *American Mineralogist*, **99**, 1724–1735.

Dazas, B., Lanson, B., Delville, A., Robert, J., Komarneni, S., Michot, L.J., and Ferrage, E. (2015) Influence of tetrahedral layer charge on the organization of interlayer water and ions in synthetic Na-saturated smectites. *Journal of Physical Chemistry C*, **119**, 4158–4172.

de la Calle, C. and Suquet, H. (1988) Vermiculite. Pp. 455–496 in: *Hydrous Phyllosilicates (Exclusive Of Micas)* (S.W. Bailey, editor). Reviews in Mineralogy, **19**. Mineralogical Society of America, Chantilly, Virginia, USA.

Delville, A. (1991) Modeling the clay-water interface. *Langmuir*, **7**, 547–555.

Delville, A. (1993) Structure and properties of confined liquids: A molecular model of the clay-water interface. *Journal of Physical Chemistry*, **97**, 9703–97102.

Drits, V., Srodon, J., and Eberl, D.D. (1997a) XRD measurement of mean crystallite thickness of illite and illite/smectite: Reappraisal of the Kubler index and the Scherrer equation. *Clays and Clay Minerals*, **45**, 461–475.

Drits, V.A., Sakharov, B.A., Lindgreen, H., and Salyn, A. (1997b) Sequential structure transformation of illite-smectite-vermiculite during diagenesis of Upper Jurassic shales from the North Sea and Denmark. *Clay Minerals*, **32**, 351–371.

Drits, V.A. and Tchoubar, C. (1990) *X-ray Diffraction by Disordered Lamellar Structures: Theory and Applications to Microdivided Silicates and Carbons*. Springer-Verlag, Berlin, 371 pp.

Dzene, L., Tertre, E., Hubert, F., and Ferrage, E. (2015) Nature of the sites involved in the process of cesium desorption from vermiculite. *Journal of Colloid and Interface Science*, **455**, 254–260.

Ferrage, E., Lanson, B., Sakharov, B.A., and Drits, V.A. (2005a) Investigation of smectite hydration properties by modeling experimental X-ray diffraction patterns: Part I. Montmorillonite hydration properties. *American Mineralogist*, **90**, 1358–1374.

Ferrage, E., Lanson, B., Malikova, N., Plançon, A., Sakharov, B.A., and Drits, V.A. (2005b) New insights on the distribution of interlayer water in bi-hydrated smectite from X-ray diffraction profile modeling of 00*l* reflections. *Chemistry of Materials*, **17**, 3499–3512.

Ferrage, E., Tournassat, C., Rinnert, E., and Lanson, B. (2005c) Influence of pH on the interlayer cationic composition and hydration state of Ca-montmorillonite: Analytical chemistry, chemical modelling and XRD profile modelling study. *Geochimica et Cosmochimica Acta*, **69**, 2797–2812.

Ferrage, E., Lanson, B., Sakharov, B.A., Geoffroy, N., Jacquot, E., and Drits, V.A. (2007a) Investigation of dioctahedral smectite hydration properties by modeling of X-ray diffraction profiles: Influence of layer charge and charge location. *American Mineralogist*, **92**, 1731–1743.

Ferrage, E., Kirk, C.A., Cressey, G., and Cuadros, J. (2007b) Dehydration of Ca-montmorillonite at the crystal scale. Part I: Structure evolution. *American Mineralogist*, **92**, 994–1006.

Ferrage, E., Lanson, B., Michot, L.J., and Robert, J. (2010) Hydration properties and interlayer organization of water and ions in synthetic Na-smectite with tetrahedral layer charge. Part 1. Results from X-ray diffraction profile modeling. *Journal of Physical Chemistry C*, **114**, 4515–4526.

Ferrage, E., Sakharov, B.A., Michot, L.J., Delville, A., Bauer, A., Lanson, B., Grangeon, S., Frapper, G., Jiménez-Ruiz, M., and Cuello, G.J. (2011a) Hydration properties and interlayer organization of water and ions in synthetic Na-smectite with tetrahedral layer charge. Part 2. Toward a precise coupling between molecular simulations and diffraction data. *Journal of Physical Chemistry C*, **115**, 1867–1881.

Ferrage, E., Vidal, O., Mosser-Ruck, R., Cathelineau, M., and Cuadros, J. (2011b) A reinvestigation of smectite illitization in experimental hydrothermal conditions: Results from X-ray diffraction and transmission electron microscopy. *American Mineralogist*, **96**, 207–223.

Fripiat, J.J., Cruz, M.I., Bohor, B.F., and Thomas, J. Jr (1974) Interlamellar adsorption of carbon dioxide by smectites. *Clays and Clay Minerals*, **22**, 23–30.

Gates, W.P., Bouazza, A., and Churchman, G.J. (2009) Bentonite clay keeps pollutants at bay. *Elements*, **5**, 105–110.

Gieseking, J.E. (1939) The mechanism of cation exchange in the montmorillonite-beidellite-nontronite type of clay minerals. *Soil Science*, **47**, 1–14.

Giesting, P., Guggenheim, S., Koster van Groos, A.F., and Busch, A. (2012a) X-ray diffraction study of K- and Ca-exchanged montmorillonites in CO_2 atmospheres. *Environmental Science and Technology*, **46**, 5623–5630.

Giesting, P., Guggenheim, S., Koster van Groos, A.F., and Busch, A. (2012b) Interaction of carbon dioxide with Na-exchanged montmorillonite at pressures to 640 bars: Implications for CO_2 sequestration. *International Journal of Greenhouse Gas Control*, **8**, 73–81.

Glaeser, R. and Méring, J. (1954) Isothermes dhydratation des montmorillonites bi-ioniques (Ca, Na). *Clay Mineral Bulletin*, **2**, 188–193.

Glaeser, R. and Méring, J. (1968) Domaines dhydratation des

https://doi.org/10.1346/CCMN.2016.0640401 Published online by Cambridge University Press

smectites. *Comptes-Rendus de lAcadémie des Sciences de Paris*, **267**, 463–466.

Glaeser, R., Mantine, I., and Méring, J. (1967) Observations sur la beidellite. *Bulletin du Groupe Français des Argiles*, **19**, 125–130.

Gruner, J.W. (1932) Crystal structure of kaolinite. *Zeitschrift für Kristallographie*, **83**, 75–88.

Gruner, J.W. (1934) The structures of vermiculites and their collapse by dehydration. *American Mineralogist*, **19**, 557–575.

Guinier, A. (1964) *Théorie et Technique de la radiocristallographie*. Dunod, Paris, 740 pp.

Harris, G.L., Nicholls, P.H., Bailey, S.W., Howse, K.R., and Mason, D.J. (1994) Factors influencing the loss of pesticides in drainage from a cracking clay soil. *Journal of Hydrology*, **159**, 235–253.

Heinz, H., Koerner, H., Anderson, K.L., Vaia, R.A., and Farmer, B.L. (2005) Force field for mica-type silicates and dynamics of octadecylammonium chains grafted to montmorillonite. *Chemistry of Materials*, **17**, 5658–5669.

Heinz, H., Lin, T., Mishra, R., and Emami, F.S. (2013) Thermodynamically consistent force fields for the assembly of inorganic, organic, and biological nanostructures: The INTERFACE force field. *Langmuir*, **29**, 1754–1765.

Hendricks, S. and Teller, E. (1942) X-ray interference in partially ordered layer lattices. *Journal of Chemical Physics*, **10**, 147–167.

Hendricks, S.B. and Fry, W.H. (1930) The results of X-Ray and microscopical examinations of soil colloids. *Soil Science*, **29**, 457–480.

Hendricks, S.B. and Jefferson, M.E. (1938) Structures of kaolin and talc-pyrophyllite hydrates and their bearing on water sorption of the clays. *American Mineralogist*, **23**, 863–875.

Hendricks, S.B., Nelson, R.A., and Alexander, L.T. (1940) Hydration mechanism of the clay mineral montmorillonite saturated with various cations 1. *Journal of the American Chemical Society*, **62**, 1457–1464.

Hofmann, U. and Bilke, W. (1936) Über die innerkristalline Quellung und das basenaustauschvermogen des montmorillonits. *Kolloid-Zeitschrift*, **77**, 238–251.

Hofmann, U., Endell, K., and Wilm, D. (1933) Kristallstruktur und quellung von Montmorillonit (Das Tonmineral der Bentonittone). *Zeitschrift für Kristallographie*, **86**, 340–348.

Holmboe, M., Wold, S., and Jonsson, M. (2012) Porosity investigation of compacted bentonite using XRD profile modeling. *Journal of Contaminant Hydrology*, **128**, 19–32.

Howard, S.A. and Preston, K.D. (1989) Profile fitting of powder diffraction patterns. Pp. 217–275 in: *Modern Powder Diffraction* (D.L. Bish and J.E. Post, editors). Reviews in Mineralogy, **20**. Mineralogical Society of America, Washington DC.

Hubert, F., Caner, L., Meunier, A., and Ferrage, E. (2012) Unraveling complex <2 μm clay mineralogy from soils using X-ray diffraction profile modeling on particle-size sub-fractions: Implications for soil pedogenesis and reactivity. *American Mineralogist*, **97**, 384–398.

Inoue, A., Lanson, B., Marques-Fernandes, M., Sakharov, B.A., Murakami, T., Meunier, A., and Beaufort, D. (2005) Illite-smectite mixed-layer minerals in the hydrothermal alteration of volcanic rocks: I. One-dimensional XRD structure analysis and characterization of component layers. *Clays and Clay Minerals*, **53**, 423–439.

Iwasaki, T. and Watanabe, T. (1988) Distribution of Ca and Na ions in dioctahedral smectites and interstratified dioctahedral mica/smectites. *Clays and Clay Minerals*, **36**, 73–82.

Lanson, B. (2011) Modelling of X-ray diffraction profiles: Investigation of defective lamellar structure crystal chemistry. Pp. 151-202 in: *Bulk and Surface Structures of Layer Silicates and Oxides: Theoretical Aspects and Applications* (M.F. Brigatti and A. Mottana, editors). EMU Notes in Mineralogy **11**, European Mineralogical Union.

Lanson, B., Sakharov, B.A., Claret, F., and Drits, V.A. (2009) Diagenetic smectite-to-illite transition in clay-rich sediments: A reappraisal of X-ray diffraction results using the multi-specimen method. *American Journal of Science*, **309**, 476–516.

Lanson, B., Ferrage, E., Hubert, F., Prêt, D., Mareschal, L., Turpault, M., and Ranger, J. (2015) Experimental aluminization of vermiculite interlayers: An X-ray diffraction perspective on crystal chemistry and structural mechanisms. *Geoderma*, **249–250**, 28–39.

Lindgreen, H., Drits, V.A., Sakharov, B.A., Jakobsen, H.J., Salyn, A.L., Dainyak, L.G., and Krøyer, H. (2002) The structure and diagenetic transformation of illite-smectite and chlorite-smectite from North Sea Cretaceous-Tertiary chalk. *Clay Minerals*, **37**, 429–450.

Madsen, F.T. (1998) Clay mineralogical investigations related to nuclear waste disposal. *Clay Minerals*, **33**, 109–129.

Maegdefrau, E. and Hofmann, U. (1937) Die Kristalstruktur des montmorillonits. *Zeitschrift für Kristallographie*, **98**, 299–323.

Marshall, C.E. (1935) Layer lattices and base-exchange clays. *Zeitschrift für Kristallographie*, **91**, 433–449.

Martins, M.L., Gates, W.P., Michot, L., Ferrage, E., Marry, V., and Bordallo, H.N. (2014) Neutron scattering, a powerful tool to study clay minerals. *Applied Clay Science*, **96**, 22–35.

McCarty, D.K., Sakharov, B.A., and Drits, V.A. (2008) Early clay diagenesis in Gulf Coast sediments: New insights from XRD profile modeling. *Clays and Clay Minerals*, **56**, 359–379.

McCarty, D.K., Sakharov, B.A., and Drits, V.A. (2009) New insights into smectite illitization: A zoned K-bentonite revisited. *American Mineralogist*, **94**, 1653–1671.

Méring, J. (1946) On the hydration of montmorillonite. *Transactions of the Faraday Society*, **42**, B205–B219.

Méring, J. (1949) L'interférence des rayons X dans les systèmes à stratification désordonée. *Acta Crystallographica*, **2**, 371–377.

Méring, J. and Glaeser, R. (1954) Sur le rôle de la valence des cations échangeables dans la montmorillonite. *Bulletin de la Société Francaise de Minéralogie et Cristallographie*, **77**, 519–530.

Michels, L., Fossum, J.O., Rozynek, Z., Hemmen, H., Rustenberg, K., Sobas, P.A., Kalantzopoulos, G.N., Knudsen, K.D., Janek, M., Plivelic, T.S., and da Silva, G.J. (2015) Intercalation and retention of carbon dioxide in a smectite clay promoted by interlayer cations. *Scientific Reports*, **5**, 8775.

Michot, L.J., Ferrage, E., Jiménez-Ruiz, M., Boehm, M., and Delville, A. (2012) Anisotropic features of water and ion dynamics in synthetic Na- and Ca-smectites with tetrahedral layer charge. A combined quasi-elastic neutron-scattering and molecular dynamics simulations study. *Journal of Physical Chemistry C*, **116**, 16619–16633.

Möller, M.W., Hirsemann, D., Haarmann, F., Senker, J., and Breu, J. (2010) Facile scalable synthesis of rectorites. *Chemistry of Materials*, **22**, 186–196.

Moore, D.M. and Hower, J. (1986) Ordered interstratification of dehydrated and hydrated Na-smectite. *Clays and Clay Minerals*, **34**, 379–384.

Moore, D.M. and Reynolds, R.C. Jr. (1997) *X-ray Diffraction and the Identification and Analysis of Clay Minerals*. Oxford University Press, New York, 322 pp.

Nagelschmidt, G. (1936) On the lattice shrinkage and structure of montmorillonite. *Zeitschrift für Kristallographie*, **93**, 481–487.

Pezerat, H. (1967) Recherches sur la position des cations échangeables et de l'eau dans les montmorillonites. *Comptes-Rendus de lAcadémie des Sciences de Paris*, **265**, 529–532.

Pezerat, H. and Méring, J. (1958) Détection des cations échangeable de la montmorillonite par l'emploi des séries différences. *Bulletin du Groupe Français des Argiles*, **10**, 25–26.

Prêt, D., Ferrage, E., Tertre, E., Pelletier, M., Robinet, J.C., Faurel, M., Bihannic, I., and Hubert, F. (2013) X-ray tomography and impregnation methods to analyze pore space heterogeneities at the hydrated state. Pp. 75–83 in: *Proceeding of the Workshop of the Nuclear Energy Agency Clayclub Clay Characterisation from Nanoscopic to Microscopic Resolution.* Karlsruhe, 6-8 September, NEA/RWM/CLAYCLUB, OECD-NEA Press, Karlsruhe.

Reynolds, R.C. Jr. (1965) An X-ray study of ethylene glycol-montmorillonite complex. *American Mineralogist*, **50**, 990, 1001.

Reynolds, R.C. Jr. (1967) Interstratified clay systems: Calculation of the total one-dimensional diffraction function. *American Mineralogist*, **52**, 661–672.

Reynolds, R.C. Jr. (1968) The effect of particle size on apparent lattice spacings. *Acta Crystallographica Section A*, **24**, 319–320.

Reynolds, R.C. Jr. (1985) *NEWMOD: A Computer Program for the Calculation of One-Dimensional Patterns of Mixed-Layered Clays.* RC Reynolds, Hanover, NH.

Reynolds, R.C. Jr. (1986) The Lorentz-polarization factor and preferred orientation in oriented clay aggregates. *Clays and Clay Minerals*, **34**, 359–367.

Reynolds, R.C. Jr. (1989) Diffraction by small and disordered crystals. Pp. 145–182 in: *Modern Powder Diffraction* (D.A. Bish and J.E. Post, editors). Reviews in Mineralogy, **20**. Mineralogical Society of America, Washington, DC.

Ross, M. (1968) X-ray diffraction effects by non-ideal crystals of biotite, muscovite, montmorillonite, mixed-layer clays, graphite, and periclase. *Zeitschrift für Kristallographie*, **126**, 80–97.

Sakharov, B.A. and Drits, V.A. (1973) Mixed-layer kaolinite-montmorillonite: A comparison of observed and calculated diffraction patterns. *Clays and Clay Minerals*, **21**, 15–17.

Sakharov, B.A. and Lanson, B. (2013) X-ray identification of mixed-layer structures. Modelling of diffraction effects. Pp. 51–135 in: *Handbook of Clay Science. Developments in Clay, 2nd ed. Part B: Techniques and Applications* **5B** (F. Bergaya and G. Lagaly, editors). Science and Publishing House, Elsevier, Amsterdam.

Sakharov, B.A., Naumov, A.S., and Drits, V.A. (1982a) X-ray diffraction by mixed-layer structures with random distribution of stacking faults. *Doklady Akademii Nauk SSSR*, **265**, 339–343.

Sakharov, B.A., Naumov, A.S., and Drits, V.A. (1982b) X-ray intensities scattered by layer structure with short range ordering parameters S>1 and G>1. *Doklady Akademii Nauk SSSR*, **265**, 871–874.

Sakharov, B.A., Lindgreen, H., Salyn, A., and Drits, V.A. (1999) Determination of illite-smectite structures using multispecimen X-ray diffraction profile fitting. *Clays and Clay Minerals*, **47**, 555–566.

Sato, T., Watanabe, T., and Otsuka, R. (1992) Effects of layer charge, charge location, and energy change on expansion properties of dioctahedral smectites. *Clays and Clay Minerals*, **40**, 103–113.

Sato, T., Murakami, T., and Watanabe, T. (1996) Change in layer charge of smectites and smectite layers in illite/smectite during diagenetic alteration. *Clays and Clay Minerals*, **44**, 460–469.

Shashikala, H.D., Suryanarayana, S.V., and Nagender Naidu, S.V. (1993) Debye temperature and mean-square amplitudes of vibration of Ti_3Al alloys. *Journal of Applied Crystallography*, **26**, 602–605.

Skipper, N.T., Refson, K., and McConnell, J.D.C. (1989) Computer calculation of water-clay interactions using atomic pair potentials. *Clay Minerals*, **24**, 411–425.

Skipper, N.T., Refson, K., and McConnell, J.D.C. (1991) Computer simulation of interlayer water in 2:1 clays. *Journal of Chemical Physics*, **94**, 7434–7445.

Skipper, N.T., Chang, F.R.C., and Sposito, G. (1995) Monte Carlo simulation of interlayer molecular structure in swelling clay minerals. 1. Methodology. *Clays and Clay Minerals*, **43**, 285–293.

Smith, D.E. (1998) Molecular computer simulations of the swelling properties and interlayer structure of cesium montmorillonite. *Langmuir*, **14**, 5959–5967.

Stanjek, H. (2002) XRD peak migration and apparent shift of cell-edge lengths of nano-sized hematite, goethite and lepidocrocite. *Clay Minerals*, **37**, 629–638.

Striolo, A. (2011) From interfacial water to macroscopic observables: A review. *Adsorption Science & Technology*, **29**, 211–258.

Suquet, H. and Pezerat, H. (1987) Parameters influencing layer stacking types in saponite and vermiculite: A review. *Clays and Clay Minerals*, **35**, 353–362.

Szczerba, M., Kłapyta, Z., and Kalinichev, A. (2014) Ethylene glycol intercalation in smectites. Molecular dynamics simulation studies. *Applied Clay Science*, **91**, 87–97.

Tertre, E., Prêt, D., and Ferrage, E. (2011a) Influence of the ionic strength and solid/solution ratio on Ca(II)-for-Na^+ exchange on montmorillonite. Part 1: Chemical measurements, thermodynamic modeling and potential implications for trace elements geochemistry. *Journal of Colloid and Interface Science*, **353**, 248–256.

Tertre, E., Prêt, D., and Ferrage, E. (2011b) Influence of the ionic strength and solid/solution ratio on Ca(II)-for-Na^+ exchange on montmorillonite. Part 2: Understanding the effect of the m/V ratio. Implications for pore water composition and element transport in natural media. *Journal of Colloid and Interface Science*, **363**, 334–347.

Tessier, D., Bouzigues, B., Favrot, J.C., and Valles, V. (1992) Influence of decimetric microrelief on clay texture evolution of hydromorphic soils of the Garonne River-differentiation of vertic and prismatic structures. *Comptes Rendus de l'Académie des sciences Paris Série II*, **315**, 1027–1032.

Trunz, V. (1976) Influence of crystallite size on apparent basal spacing of kaolinite. *Clays and Clay Minerals*, **24**, 84–87.

Ufer, K., Kleeberg, R., Bergmann, J., and Dohrmann, R. (2012) Rietveld refinement of disordered illite-smectite mixed-layer structures by a recursive algorithm. I. One-dimensional patterns. *Clays and Clay Minerals*, **60**, 507–534.

Vasseur, G., Djeran-Maigre, I., Grunberger, D., Rousset, G., Tessier, D., and Velde, B. (1995) Evolution of structural and physical parameters of clays during experimental compaction. *Marine and Petroleum Geology*, **12**, 941–954.

Viennet, J., Hubert, F., Ferrage, E., Tertre, E., Legout, A., and Turpault, M. (2015) Investigation of clay mineralogy in a temperate acidic soil of a forest using X-ray diffraction profile modeling: Beyond the HIS and HIV description. *Geoderma*, **241–242**, 75–86.

Waasmaier, D. and Kirfel, A. (1995) New analytical scattering-factor functions for free atoms and ions. *Acta Crystallographica Section A*, **51**, 416–431.

Yang, N. and Yang, X. (2011) Molecular simulation of swelling and structure for Na-Wyoming montmorillonite in supercritical CO_2. *Molecular Simulation*, **37**, 1063–1070.

(*Received 29 September 2015; revised 21 March 2016; Ms. 1040; AE: A.G. Kalinichev*)